

Nature's most squishy ion: The important role of solvent polarization in the description of the hydrated electron

John M. Herbert* and Leif D. Jacobson

Department of Chemistry, The Ohio State University, Columbus, OH 43210

(Received 12 July 2010; final version received 18 October 2010)

The aqueous electron, $e^-(aq)$, and its finite analogues, the anionic water clusters $(H_2O)_n^-$, have attracted significant attention from both theory and experiment over the past few decades. Nevertheless, some of the most basic structural aspects of these systems, as well as the interpretation of certain spectroscopic features, remain controversial or else have defied theoretical explanation altogether. Due to the solvent-supported nature of the ion, a large number of water molecules is required in order to obtain a realistic model of $e^-(aq)$, and a wide variety of structural morphologies are available in $(H_2O)_n^-$ clusters. These aspects severely limit the role of *ab initio* quantum chemistry in elucidating the properties of solvated-electron systems, but at the same time, the fundamentally quantum-mechanical nature of the ion must be taken into account. Most theoretical studies have therefore relied upon one-electron pseudopotential models and mixed quantum/classical molecular dynamics. In view of the highly diffuse, polarizable nature of the ion, however, it is surprising how little attention has been paid to the development of polarizable one-electron models. This article presents an overview of our efforts to develop such a model, as well as computational evidence to suggest that self-consistent, many-body electron–water polarization is *qualitatively* important in the description of both $(H_2O)_n^-$ clusters and $e^-(aq)$ in bulk water.

Keywords: aqueous electron; solvated electron; quantum/classical molecular dynamics; polarization

	PAGE
1. Introduction	2
1.1. Historical background	2
1.2. Electron binding motifs in clusters	3
1.3. Open questions regarding the bulk species	7
1.4. Motivation for the present approach	8
2. Why bother with a polarizable model?	10
2.1. Is a one-electron model even appropriate?	10
2.1.1. Indications of many-electron character	12
2.1.2. Many-electron calculation of the optical spectrum of $e^-(aq)$	13
2.2. Correlation and localization in clusters	16

*Corresponding author. Email: herbert@chemistry.ohio-state.edu

2.3. Shortcomings of simple water models	19
3. The delicate business of constructing a pseudopotential	22
3.1. Some non-heuristic procedures	23
3.2. Our own efforts: PEWP-1 and PEWP-2	26
3.2.1. PEWP-1: Success for clusters, failure for bulk $e^-(aq)$	26
3.2.2. PEWP-2: A new approach	29
4. The role of polarization in the bulk species, $e^-(aq)$	32
4.1. Vertical electron binding energy	32
4.2. Excited electronic states	35
5. Summary	40
Acknowledgements	41
References	42

1. Introduction

1.1. Historical background

The notion of a “solvated electron” was introduced more than a century ago, in order to explain the electrical conductance [1–4] and optical spectra [5] exhibited by solutions of alkali metals in various solvents. As early as 1952, it had been suggested that such a species might be a byproduct of the radiolysis of aqueous solutions [6,7], but owing to the relatively short lifetime ($\sim 10^{-5}$ s) of solvated electrons in water [8], the existence of the aqueous electron, $e^-(aq)$, was not confirmed until 1962 [9,10] when its optical spectrum was observed in a pulsed radiolysis experiment.¹ In subsequent decades, $e^-(aq)$ has come to be recognized as one of the primary radicals formed upon radiolysis of water [11,14–16] and short-lived excited states of this species have been implicated in biological radiation damage [17–20].

From the standpoint of theoretical chemical physics, the solvated electron is perhaps *the* prototypical system for studying the interplay between quantum mechanics (which is required in order to describe the unpaired “excess” electron) and the statistical mechanics and dynamics of condensed media or clusters. In many solvents, the existence of a “solvated electron” is solely a result of cooperative, many-body interactions within the solvent, since an individual solvent molecule may not bind an extra electron. (The H_2O^- ion does not exist, for example; at least two water molecules are required in order to obtain a non-zero electron binding energy [21].)

As path integral methods became fashionable in the 1980s [22], solvated electrons (in water, methanol, ammonia, alkyl amines, and molten salts) quickly became the “go-to” systems for exploring such approaches [23–42]. These early simulations were based upon rather heuristic electron–water interaction potentials [27,29,30] and crude water force fields, at least by modern standards, and were concerned mainly with demonstrating that the electron does indeed localize in polar condensed media. Around this same time, $(\text{H}_2\text{O})_n^-$ cluster anions, the finite-size analogues of $e^-(aq)$, were first produced and detected in the gas phase [43], and path-integral calculations were subsequently used to demonstrate

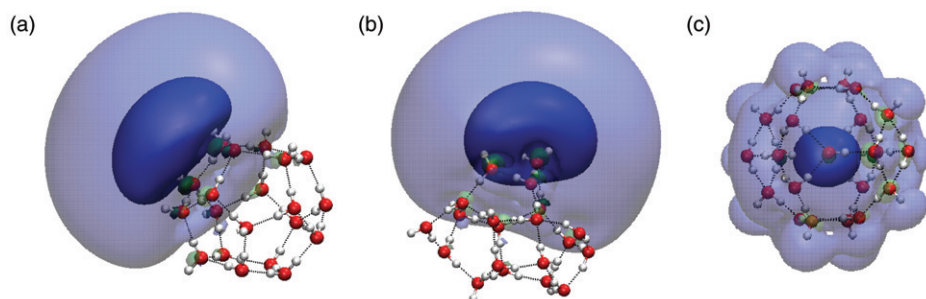


Figure 1 (colour online). Examples of electron-binding motifs in water cluster anions: (a) a surface state of $(\text{H}_2\text{O})_{20}^-$, in which one O–H moiety from each of four water molecules is coordinated to the electron; (b) a surface state of $(\text{H}_2\text{O})_{20}^-$ that exhibits the “double acceptor” (“AA”) binding motif, in which a single water has both H atoms coordinated to the electron; and (c) a cavity state of $(\text{H}_2\text{O})_{24}^-$, in which four water molecules in the first solvation shell each have one O–H moiety coordinated to the electron. The electronic wavefunction in these images is the singly-occupied molecular orbital (SOMO) computed at the Hartree-Fock/6-31(1+,3+)G* level [44], and the opaque and translucent isosurfaces represent 50% and 95% isoprobability contours, respectively. Note the small green lobes situated near the water molecules, which have opposite sign from the main lobes that are shown in blue.

that more than one electron-binding motif may exist at a given cluster size [39,41]. In particular, both surface-bound as well as internalized (cavity-bound) electron-binding motifs were predicted by the simulations. Illustrative examples of these binding motifs are depicted in Figure 1.

Early on, it was recognized that the results of these path-integral simulations were rather sensitive to the details of the electron–water interaction potential [26], and therefore attempts were made to incorporate effects such as local (scalar) exchange and local kinetic energy enhancement [37], and to develop entirely *ab initio* prescriptions for determining an interaction potential [45,46]. Focusing on aqueous solvation alone, a large number of electron–water interaction potentials have been proposed over the past 25 years [27,29,30,37,45,47–56] and an even larger number of simulations have been based on these one-electron models [24–42,47–51,53,56–80]. As such, an outsider might reasonably question whether there is anything left to learn about electrons in water! However, despite a quarter-century of detailed simulations, and a wealth of experimental data for both $(\text{H}_2\text{O})_n^-$ clusters and bulk $e^-(aq)$, many basic questions remain unanswered regarding the structure, dynamics, and spectroscopy of this diffuse, polarizable, and fundamentally quantum-mechanical solute.

1.2. Electron binding motifs in clusters

One of the most contentious questions over the past twenty years has been the nature of the electron binding motif in $(\text{H}_2\text{O})_n^-$ clusters [81]. This controversy dates back to 1990, when the first photo-electron spectra of size-selected water cluster anions ($n = 2–69$) were reported by Bowen and co-workers [82,83]. From these spectra, one obtains the vertical electron binding energy (VEBE),

$$\text{VEBE} = E_{\text{neutral}} - E_{\text{anion}}, \quad (1)$$

as a function of cluster size, n . VEBEs obtained from these and other experiments are plotted in Figure 2.

In many cases, one can identify more than one VEBE at a given cluster size, presumably indicative of the existence of different cluster isomers exhibiting different electron binding motifs. For $n \gtrsim 11$, the ‘‘Isomer I’’ VEBE data in Figure 2 extrapolate approximately linearly as a function of $n^{-1/3}$, albeit with an apparent change in slope around $n \sim 30$ [81]. Assuming a roughly spherically cluster, this indicates that the VEBE scales as the inverse cluster radius, which is what one expects for an electron in a cavity, based on simple Born-type continuum solvation models [40,91,92]. (Other properties, such as the electronic absorption line shape [90,93] and electronic relaxation lifetimes [94,95] also extrapolate smoothly, though the latter appear to be linear with respect to n^{-1} , rather than $n^{-1/3}$.) At the time, this observation was taken as evidence that, for $n > 11$, the electron is internalized within the cluster, forming a so-called cavity-bound cluster isomer, akin to that depicted for $(\text{H}_2\text{O})_{24}^-$ in Figure 1(c). (This particular structure was constructed for purposes of illustration only; the task of identifying the precise cluster structures that

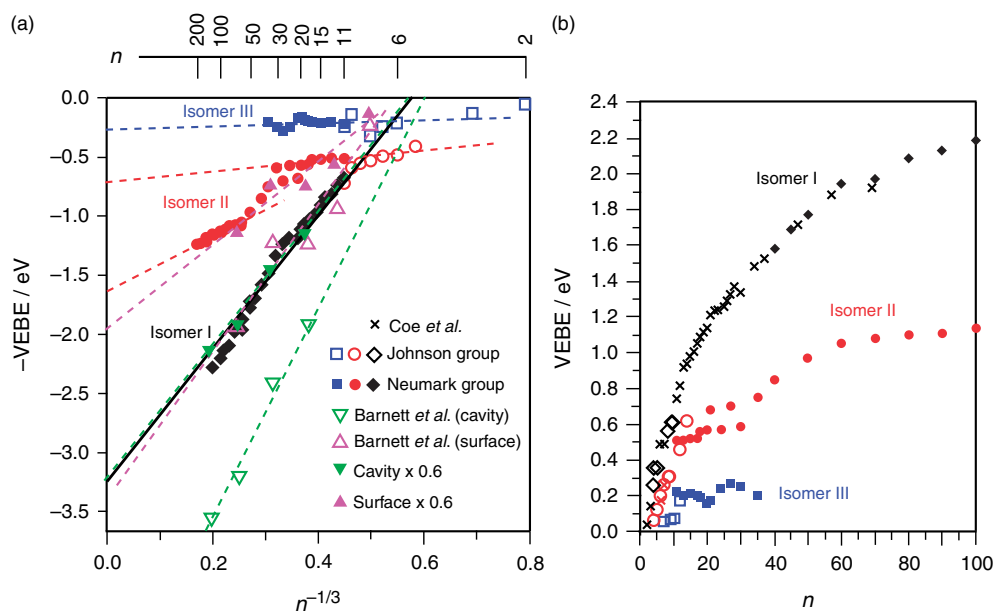


Figure 2 (colour online). Vertical electron binding energies (VEBEs) for size-selected $(\text{H}_2\text{O})_n^-$ clusters. Experimental values from Coe *et al.* [82] (Bowen group) and from Verlet *et al.* [84] (Neumark group) were measured via photo-electron spectroscopy, whereas data from Johnson and co-workers [85–87] were measured mostly using infrared argon predissociation spectroscopy. Theoretical values were calculated by Barnett *et al.* [39], using a one-electron pseudopotential model [88]. Also shown are these same theoretical values, scaled by an *ad hoc* factor of 0.6 that was chosen [84] in order to bring the calculations in line with experimental data for Isomers I and II. Experimentally, no isomers are found at higher VEBEs than the Isomer I data series [89]. The solid black line in (a) represents the extrapolation reported by Coe *et al.* [90], based on data for $n = 2$ –69, whereas the broken lines are merely guides for the eye. [Panel (a) was adapted from Ref. [84]; repeated with permission from AAAS. Panel (b) was adapted from Ref. [87]; copyright 2005 American Chemical Society.]

are seen experimentally is a difficult one, which we defer here.) In a subsequent analysis of these same photo-electron data, the smaller of these Isomer I clusters were termed “bulk embryonts” [90,93]. This term is appropriate, given that clusters smaller than $n \sim 20$ probably cannot fully encapsulate the electron in a manner that one would deem analogous to a cavity-bound electron in liquid water [see Figure 1(c)]. Assuming that the Isomer I data in Figure 2 do indeed represent cavity-bound $(\text{H}_2\text{O})_n^-$ isomers, extrapolation of the cluster data [90] affords an estimate of 3.4 eV for the VEBE of $e^-(aq)$ in bulk water, in reasonable agreement with values reported recently based on liquid microjet experiments [96–98]. Extrapolations based on data for very cold $(\text{H}_2\text{O})_n^-$ clusters, however, suggest a somewhat larger value for the bulk VEBE [99].

The assignment of the photo-electron spectra to cavity-bound cluster isomers was controversial from the start, due to prior theoretical calculations of cluster VEBEs by Barnett *et al.* [38–41] that proved to be in remarkably good agreement with the experimental data for what is now termed the “Isomer I” series, but for *surface-bound* cluster isomers; see Figure 2(a). According to the calculations, cavity-bound isomers exhibit systematically larger VEBEs as a function of n . These calculations were based on a one-electron pseudopotential model [88], and it has been suggested that this particular pseudopotential may overbind the excess electron [100,101]. Recently, however, results quite similar to those obtained by Barnett *et al.* were reported [78] using a newer one-electron model [49]. On the other hand, experiments in which the photodetachment laser is tuned to 4.7 eV show no sign of isomers whose VEBEs are larger than the Isomer I data [89].

In 2005, Verlet *et al.* [84] demonstrated the existence of at least two additional series of isomers with significantly lower VEBEs. These isomers, labeled “Isomer II” and “Isomer III” in Figure 2, appear only at lower temperatures, and were not seen in the earlier photo-electron experiments by Bowen and co-workers [82,83]. Verlet *et al.* assigned them to surface-bound isomers of the excess electron. This interpretation is bolstered by the observation [84] that *ad hoc* scaling of the 1980s-era VEBE calculations of Barnett *et al.* [39] brings the surface-bound calculations into reasonable agreement with the experimental data for Isomer II, and simultaneously brings the cavity-bound calculations into decent agreement with the Isomer I data.

In a separate set of experiments [102,103] Neumark and co-workers measured time-resolved VEBEs for $\text{I}^-(\text{H}_2\text{O})_n$ clusters ($n=3-28$) following excitation of the charge-transfer-to-solvent (CTTS) band, which ultimately forms a solvated electron. At early pump/probe delay times, the VEBEs were found to be in good agreement with the Isomer II data in Figure 2, but these VEBEs increase as a function of time, ultimately coming into agreement with the Isomer I data at longer delay times [81]. This is significant, given that I^- is believed to bind at the surface of water clusters, hence CTTS excitation is expected to prepare a surface-bound electron initially, which might internalize at later times.

The calculations by Barnett *et al.* [39] predict that the thermodynamic transition from surface states to internal states occurs between $n=32$ and $n=64$, rather than $n \sim 11$ as one might infer from the photo-electron data, under the assumption that the Isomer I data represent cavity-bound isomers. Calculations by Turi *et al.* [73], using a newer one-electron pseudopotential model [49], suggest that the transition occurs later still, around $n \sim 200$ at $T=150$ K, and it has been suggested that the photo-electron experiments likely probe metastable isomers, so that extrapolation of these data to the bulk limit is not appropriate [104].

Other aspects of the n -dependent evolution of $(\text{H}_2\text{O})_n^-$ morphology also remain poorly understood. In small clusters ($n \leq 7$), vibrational [87,105–108] and photo-electron spectra [85,86] have been definitively assigned to particular cluster isomers, on the basis of *ab initio* calculations [106,107,109,110]. An interesting feature of these assignments is that the experiments—the most well-resolved of which are argon-mediated action spectra of $\text{Ar}_m \cdot (\text{H}_2\text{O})_n^-$ clusters—show a preponderance of high-VEBE isomers that calculations suggest lie many factors of $k_B T$ above the minimum-energy structures, at the estimated experimental temperature (~ 50 K for argon-tagged clusters) [70–72,110]. The high-energy isomers that are prevalent in the experimental spectra invariably exhibit the so-called double acceptor or “AA” electron binding motif [106], in which a single water molecule coordinates both of its hydrogen atoms to the excess electron. (As such, this H_2O molecule is a “double acceptor” with respect to the hydrogen-bonding network.) Figure 1(b) depicts an example of an AA isomer in $(\text{H}_2\text{O})_{20}^-$, while Figure 3(a) shows an AA isomer of $(\text{H}_2\text{O})_6^-$. The AA binding motif exhibits characteristic vibrational signatures [87,106–108,110] that persist in larger clusters [111,112], up to $n \sim 50$, where detailed *ab initio* studies are not feasible. Resonance Raman spectroscopy of $e^-(aq)$ in bulk water, however, suggests that only one hydrogen atom per H_2O molecule is coordinated to the electron [113]. Together, these observations suggest a size-dependent structural transition for some $n > 50$.

This discussion points to one of the major difficulties encountered in theoretical studies of solvated electrons: while a one-electron picture of $(\text{H}_2\text{O})_n^-$ and $e^-(aq)$ has much conceptual appeal, and also (as we shall argue herein) much practical utility, it is a mistake to consider that solvated-electron systems become “simple” upon electron detachment. The presence of the extra electron in $(\text{H}_2\text{O})_n^-$ drives the system into solvent configurations that are highly unstable in the absence of the extra electron. As such, a quantitative description of the spectroscopy of $(\text{H}_2\text{O})_n^-$ clusters demands an accurate description of *both* the $(\text{H}_2\text{O})_n^-$ potential energy surface *and* the $(\text{H}_2\text{O})_n$ potential surface, in regions that may be far from their respective global minima. Thus, gas-phase cluster studies are interesting and useful not just because they allow us to construct a molecule-by-molecule picture of solvation, but also specifically because cluster solvation is *not* like bulk solvation [114]. In clusters, the absence of an isotropic solvation environment opens the possibility of

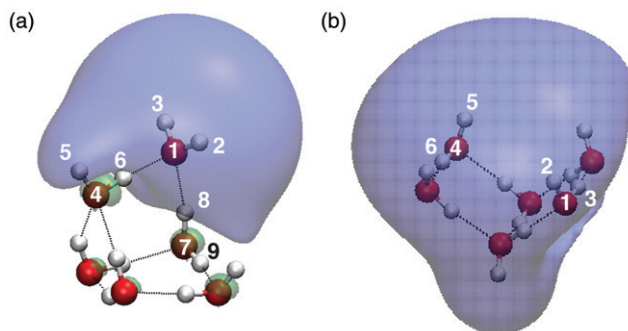


Figure 3 (colour online). Hartree-Fock/6-31(1+,3+)G* SOMOs for (a) an AA isomer of $(\text{H}_2\text{O})_6^-$ and (b) the “book” isomer of $(\text{H}_2\text{O})_6^-$. Both isosurfaces are 50% isoprobability contours, and atom labels correspond to those used later, in Table 1.

a far wider variety of structural motifs. Accurate description of the relative energetics of these various structural motifs places stringent demands on theoretical models.

1.3. Open questions regarding the bulk species

Of course, it is $e^-(aq)$ and not $(\text{H}_2\text{O})_n^-$ that is important in aqueous-phase radiation chemistry, and while development of a model that can accurately describe the structure and spectroscopy of $(\text{H}_2\text{O})_n^-$ is certainly challenging, we shall see that the description of $e^-(aq)$ is also decidedly non-trivial. Furthermore, while cluster studies have garnered much of the attention in the recent hydrated-electron literature, there are also some interesting, as-yet-unexplained observations regarding the bulk species.

In fact, even the most basic structural features of $e^-(aq)$ continue to be debated. A cavity-type picture of electron solvation, in which $e^-(aq)$ forms a quasi-spherical, *s*-like ground state within a void carved out of the solvent, has been the dominant theoretical paradigm for as long as calculations have been performed on this system [115]. Over the years, this picture has been reinforced by numerous atomistic simulations [23–36,49,116]. However, Sobolewski and Domcke have recently suggested [117–120], on the basis of high-level *ab initio* calculations on neutral $(\text{H}_3\text{O})(\text{H}_2\text{O})_n$ clusters ($n \leq 9$), that certain features of “ $e^-(aq)$ ” spectroscopy can be explained instead in terms of a neutral hydronium (H_3O) radical that, in aqueous solution, exhibits substantial zwitterionic character, and is thus solvated quite effectively.² According to this scenario, $\text{OH}^-(aq)$ might actually be responsible for the large diffusion coefficient that is attributed to $e^-(aq)$, whereas $\text{H}_3\text{O}(aq)$ is responsible for its spectroscopy [119,120]. Although this point of view remains outside of the mainstream, and is not considered further here, we find this scenario intriguing, and the calculations of Sobolewski and Domcke are by no means obviously flawed. As such, the “hydrated hydronium hypothesis” merits further investigation in larger $\text{H}_3\text{O}(\text{H}_2\text{O})_n$ clusters.

Even if we limit our attention to one-electron pseudopotential models of an excess electron in bulk water, the structure of $e^-(aq)$ is not unambiguous. Certain pseudopotential models predict a coordination number of around four [49,116] while others predict a six-coordinate structure [33]. The latter is more in line with the structure deduced by Kevan [123,124] on the basis of electron spin resonance experiments in alkaline glasses at $T = 77$ K, although the relevance of those measurements to $e^-(aq)$ in ambient liquid water is unclear. Very recently, Larsen *et al.* [56] have questioned the cavity model itself, on the basis of results obtained using a new one-electron pseudopotential that we shall discuss in Section 3. In simulations performed using this pseudopotential, the unpaired electron does not localize to the same extent that it does in all other reported calculations using one-electron pseudopotentials, although it remains an extra-valence species that inhabits the voids between water molecules.

The structure of $e^-(aq)$ is not an experimental observable *per se*, and must therefore be inferred on the basis of other measurements or theoretical calculations. In the latter case, the plausibility of a given theoretical model depends upon the extent to which it reproduces known experimental data. It is therefore noteworthy that several well-established pieces of experimental data have not yet been explained by any theoretical model or simulation. One of these is the entropy of hydration of $e^-(aq)$, which Han and Bartels [125] determined to be $\Delta S_{\text{hyd}}^\circ = +125 \text{ J mol}^{-1} \text{ K}^{-1}$, based on experimental kinetics

data [126]. To appreciate the significance of this result, consider that $\Delta S_{\text{hyd}}^{\circ} = -11 \text{ J mol}^{-1} \text{ K}^{-1}$ for the iodide anion, which has long been considered to be the most “structure-breaking” ion, in the sense of the so-called Hofmeister series [127]. (The negative value of $\Delta S_{\text{hyd}}^{\circ}$ that is measured for I^{-} is presumably attributable to the fact that the ion strongly orients the O–H bond vectors in its first solvation shell.) These observations led Han and Bartels to characterize e^{-} as the “champion structure breaker” [126].

Finally, let us mention the electronic spectroscopy of $e^{-}(aq)$. The aqueous electron was originally detected by means of its absorption in the near-infrared [9–11], and this remains the primary experimental handle for detection of this species. As such, it is significant that no theoretical model or calculation (prior to our own recent work [116,128] that is reviewed herein) has provided even a qualitatively satisfactory description of this spectrum. In particular, the asymmetric Lorentzian tail observed on the high-energy side of the spectrum [11,93,129–131] is completely absent in simulated spectra [31,34,35,49,79,132]. We have recently discovered [116,128] that this feature arises from solvent polarization following excitation of the excess electron, an effect that cannot be captured in any one-electron model, unless many-body electron–water polarization is included explicitly in the model.

1.4. Motivation for the present approach

Initially, it was not the bulk species but rather the cluster experiments described in Section 1.2 that drew us to study the hydrated electron. In our opinion, final resolution of the outstanding questions regarding the nature of $(\text{H}_2\text{O})_n^{-}$ clusters will ultimately require theoretical calculations using a method that affords an accurate description of the energy landscape for both neutral and anionic water clusters. This is what we set out to accomplish, although for reasons discussed below, our recent work has focused more on the bulk species.

It is well known that polarizable water models provide a much better description of the relative energetics of neutral water clusters, as compared to non-polarizable models [54,133–135], and we expect that the need for a polarizable water model will only increase when an extra electron is added to the system, since those water molecules nearest the electron may experience a very different electrostatic environment, as compared to water molecules that are far from the site of electron binding. A few different one-electron models for the hydrated electron have been developed that incorporate a polarizable water model [30,52,53,132], however, the only one that has been thoroughly benchmarked and extensively utilized is the so-called Drude model, developed by Jordan and co-workers [50–52,136]. This model employs a “Drude oscillator” for each water molecule (a “charge-on-a-spring” model that is a well-known way to describe dispersion interactions [137]), then treats these oscillators quantum-mechanically, along with the unpaired electron. Benchmark tests in small $(\text{H}_2\text{O})_n^{-}$ clusters demonstrate that this approach affords VEBEs that fall within $\sim 0.1 \text{ eV}$ of those obtained with high-level *ab initio* methods [52,138] including quantum Monte Carlo calculations and large-basis coupled-cluster calculations with perturbative triples [CCSD(T)]. For comparison, *ab initio* methods such as second-order Møller-Plesset perturbation theory (MP2) and *certain* density functional theory

(DFT) approaches, as discussed in Section 3.2.2,³ typically afford VEBEs within ~ 0.1 – 0.3 eV of CCSD(T) benchmarks [44,139–141] given an appropriate choice of basis set.

From all appearances, the Drude model is as accurate (at least for VEBEs) as high-level *ab initio* quantum chemistry, yet this model is affordable enough so that exhaustive structure searches have been reported for $n=6$ [72], $n=7$ [71], and $n=13$ [51], as compared to $n=4$ using *ab initio* molecular dynamics at the level of DFT [110]. However, the Drude model is significantly *more* expensive than simple one-electron pseudopotential models, since application of the Drude model to $(\text{H}_2\text{O})_n^-$ requires the solution of a $3(n+1)$ -dimensional Schrödinger equation rather than a three-dimensional Schrödinger equation. Single-point energy calculations using the Drude model have been reported for clusters as large as $n=45$ [52,142] and could probably be pushed to even larger clusters, especially if approximation techniques are applied to some of the Drude oscillators [51,52]. Nevertheless, it remains unclear whether sufficient sampling can be achieved in clusters that are *significantly* larger than $n=45$. Simulations of this sort may be necessary, given recent reports [73] that the thermodynamic surface \rightarrow internal transition occurs around $n\sim 200$ at temperatures typical of anion photo-electron experiments. Furthermore, periodic boundary conditions have yet to be implemented for the Drude model, so this model has not yet been applied to the bulk species, $e^-(aq)$.

These considerations have led us to seek a middle ground, by developing a one-electron pseudopotential model, based on a polarizable water model, that is affordable enough to be applied in bulk water with large, periodic simulation cells, yet is capable of predicting VEBEs to within ~ 0.1 – 0.2 eV, across a wide range of binding energies. This level of accuracy will allow us to make contact with cluster photo-electron experiments. At the same time, we wish to infer relationships between cluster spectroscopy and bulk measurements, since the ongoing debate regarding surface states versus cavity states of $(\text{H}_2\text{O})_n^-$ clusters is, at its core, a debate over extrapolations to the bulk limit. Thus, we also desire a model that can reproduce known properties of bulk $e^-(aq)$, including the optical absorption maximum, diffusion coefficient, and radius of gyration.

The construction of such a model, and its benchmarking against *ab initio* quantum chemistry for small clusters, is discussed in Section 3 of this review. Because $(\text{H}_2\text{O})_n^-$ clusters sample a far greater variety of morphologies than does $e^-(aq)$, we initially assumed—perhaps naïvely—that any model capable of providing accurate VEBEs and relative conformational energies in finite clusters would automatically provide an accurate description of $e^-(aq)$ in bulk water. This assumption turns out to be spectacularly false. Our initial model [54], which at the time was the most accurate one-electron model yet developed, with respect to *ab initio* cluster benchmarks, failed to localize the electron in bulk water, or to provide anything approximating realistic $e^-(aq)$ diffusion through bulk water. This contrast between cluster and bulk results points to some subtleties in the construction of an electron–water pseudopotential, the key ingredient in any one-electron model of the hydrated electron. These subtleties are discussed in Section 3.

Motivated by the failure of our original model in bulk solution, we recently revisited the construction of an electron–water pseudopotential [116]. “Version 2.0” of our polarizable, one-electron model [116] reproduces both *ab initio* benchmarks for clusters, as well as known experimental data for $e^-(aq)$. Although our original interest in the hydrated electron was piqued by cluster experiments, the poor performance of the original model for $e^-(aq)$ has led us to focus initially on the bulk species. Thus, the results that we present

here (in Section 4) focus exclusively on $e^-(aq)$. This represents the first careful analysis of the role of self-consistent polarization in this system, and we find that solvent polarization has important *qualitative* effects on both the bulk VEBE and the optical absorption spectrum of $e^-(aq)$ [116,128].

The remainder of this review is organized as follows. In Section 2, we elaborate on the theoretical considerations that lead us to believe that a polarizable model is essential in order to understand the hydrated electron. As part of this discussion, we consider whether a one-electron description of this system is indeed appropriate, and what the limitations of such a description might be. Section 3 describes various techniques for constructing an electron–water interaction potential, and our experience with them. As indicated above, parameterizing a pseudopotential is a dicey endeavor, and one should carefully benchmark any new hydrated-electron model against *both* cluster *and* bulk data. Finally, Section 4 describes our results for the bulk species using our newest model, with emphasis on the role of solvent polarization.

2. Why bother with a polarizable model?

In Sections 2.2 and 2.3, we will elaborate upon our motivation for incorporating a *polarizable* force field for the water molecules, in the context of a “simple” one-electron pseudopotential model. (Simple, that is, in comparison to the aforementioned Drude model.) First, however, we take a brief sidetrack to discuss the extent to which it is appropriate to single out just one quantum-mechanical (QM) electron in a system such as $(\text{H}_2\text{O})_n^-$.

2.1. Is a one-electron model even appropriate?

There is an undeniable intuitive appeal to one-electron models of $e^-(aq)$, which have been in use almost since the first definitive identification of this species [115]. To wit, one might expect that the singly-occupied molecular orbital (SOMO) would largely be localized in a different region of space from the valence MOs of the water molecules, so that electron–water interactions might be weak enough to be modeled using a scalar pseudopotential. Indeed, we have used this argument to explain why reasonably accurate VEBEs can be obtained at the MP2 level, and with double- ζ basis sets [44,139]: if detachment of the unpaired electron does not significantly perturb the water MOs, then any inadequacies in the description of the H_2O electronic structure will cancel when taking the difference in Equation (1), and what really matters is a reliable description of the SOMO. This can be achieved using basis sets that are highly diffuse but otherwise quite modest.

To quantify these ideas, let us define the correlation energy associated with the unpaired electron [139,140],

$$\Delta = E_{\text{corr}}(\text{neutral}) - E_{\text{corr}}(\text{anion}). \quad (2)$$

Figure 4 depicts values of Δ , obtained at the MP2 and CCSD(T) levels of theory, for various $(\text{H}_2\text{O})_n^-$ isomers ($n=2-33$) taken from databases in Refs. [139] and [140]. In most circumstances, one expects $E_{\text{corr}} \gtrsim 0.5 \text{ eV}$ per electron. For example, $E_{\text{corr}}/N_{\text{elec}} = 0.57 \text{ eV}$ for He atom [143] and $E_{\text{corr}}/N_{\text{elec}} = 0.70 \text{ eV}$ for H_2O at its equilibrium geometry, using a

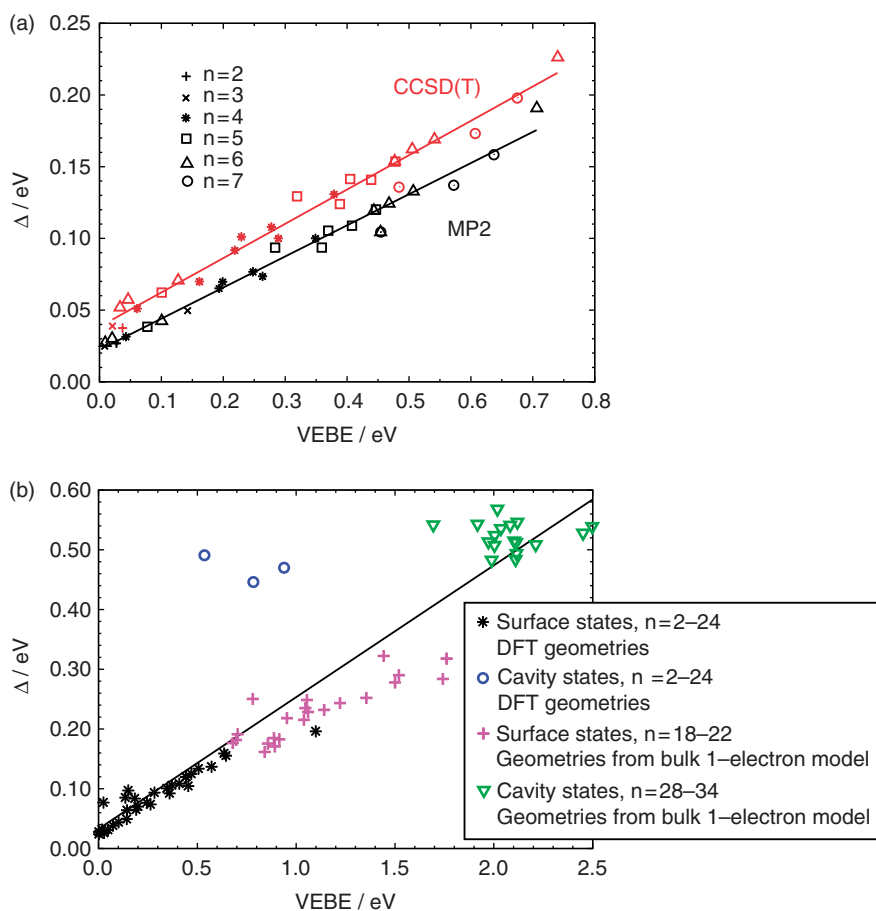


Figure 4 (colour online). Plots of the correlation energy associated with the unpaired electron [Δ , as defined in Equation (2)] versus VEBE, for various $(\text{H}_2\text{O})_n^-$ isomers: (a) MP2/ and CCSD(T)/6-31(1+,3+)G* results for small clusters ($n \leq 7$), optimized at the B3LYP/6-31(1+,3+)G* level; and (b) MP2/6-31(1+,3+)G* results for a larger set of clusters ($n \leq 33$), with geometries obtained in various ways. (See Ref. [140] for details.) The diagonal lines are obtained by linear regression analysis. (Panel (a) was adapted from Ref. [139]; copyright 2006 The Royal Society of Chemistry. A figure analogous to panel (b) but using a somewhat different data set can be found in Ref. [140].)

triple- ζ basis set [144]. However, the values of Δ that we obtain for $(\text{H}_2\text{O})_n^-$ clusters are considerably smaller than these typical values, at least when the VEBE is ≤ 1.5 eV. This suggests that the unpaired electron in these cluster isomers is only weakly correlated with the H_2O valence electrons. Only when the VEBE approaches 2 eV do we begin to obtain values of Δ comparable to valence electron correlation energies.

These data suggest that electron correlation effects for the hydrated electron are relatively weak, and might therefore reasonably be described using a one-electron pseudopotential. At the same time, one should reflect upon the 95% isoprobability contours depicted in Figure 1, which make it clear that the SOMO for a cavity-bound state has significant overlap with water molecules in both the first and second solvation shells.

In contrast, this overlap is significantly diminished for surface-bound isomers. We will return to this point in Section 2.2.

2.1.1. Indications of many-electron character

Despite the widespread use of one-electron models for hydrated-electron systems, there exists both direct and indirect experimental evidence to suggest that many-electron character is not entirely negligible. Perhaps the most direct bit of evidence emerged only recently, from Bartels and co-workers [145], who have re-measured the extinction coefficient (*i.e.*, the integrated oscillator strength) for $e^-(aq)$ in bulk water. These authors report a value of ~ 1.1 that, even in consideration of the estimated experimental uncertainty, is definitely greater than unity. The significance of this results stems from the Thomas-Reiche-Kuhn sum rule [146], which states that the sum of all oscillator strengths $f_{0 \rightarrow n}$ out of the ground state is equal to the number of electrons involved in the transition,

$$\sum_{n>0} f_{0 \rightarrow n} = N_{\text{elec}}. \quad (3)$$

In light of the result from Bartels and co-workers [145], the electronic excitations of $e^-(aq)$ must possess some many-electron character.

Other experimental data have been inferred as evidence of many-electron character, on the basis of theoretical calculations. Shkrob [147,148] has recently reviewed the magnetic resonance data for solvated electrons in water [148] and in ammonia [147], and has calculated hyperfine coupling constants for an excess electron surrounded by an idealized coordination shell of solvent molecules. The calculated coupling parameters are in qualitative agreement with those extracted from the spectra, lending credence to the calculations. Based upon Mulliken population analysis, Shkrob estimates that 10–20% of the spin density ($\rho_\alpha - \rho_\beta$) is supported by oxygen $2p$ atomic orbitals, in the case of water [148,149]. (A somewhat greater charge transfer to solvent is observed for the electron in ammonia [147].) On the other hand, one might reasonably criticize the use of Mulliken population analysis, on account of its well-known sensitivity to the presence of diffuse basis functions, which are critical in this context. Moreover, in a variational self-consistent field (SCF) calculation, there is no *a priori* reason why the oxygen $2p$ atomic orbitals should *not* contribute to the SOMO.

Natural population analysis [150], which is based upon the theory of natural bond orbitals [151], affords an atomic partition of the electron density that tends to be far more stable with respect to changes in the basis set than is Mulliken analysis [150]. We have applied this technique to analyze electron penetration in small $(\text{H}_2\text{O})_n^-$ cluster isomers, using carefully-calibrated “floating center” (“ghost atom”) basis functions to represent the unpaired electron [152]. In certain cases, these calculations predict the transfer of up to $\sim 20\%$ of the spin density from the floating center into O–H σ^* MOs, although the extent of this charge transfer is highly isomer-dependent.

Penetration of the excess electron into the σ_{OH}^* antibonding orbitals may be quantified using the difference in α - and β -spin occupation numbers for the NBOs. In Table 1 we report these differences for two isomers of $(\text{H}_2\text{O})_6^-$: an AA-type isomer, as well as the so-called book isomer, which is more closely analogous to a stable, neutral $(\text{H}_2\text{O})_6$ isomer, and contains no AA-type water molecules. (These isomers are depicted in Figure 3.) The

Table 1. The α - and β -spin occupation numbers of the O–H σ^* natural bond orbitals, for the “AA” isomer and the “book” isomer of $(\text{H}_2\text{O})_6^-$. (Structures and atom labels for these clusters are given in Figure 3.) Details of the calculations may be found in Ref. [152]. (Adapted from Ref. [152]; copyright 2006 American Chemical Society.)

Isomer	Bond	MP2			B3LYP		
		α	β	$\alpha - \beta$	α	β	$\alpha - \beta$
AA	O ₁ –H ₂	0.072	0.010	0.062	0.117	0.001	0.116
AA	O ₁ –H ₃	0.090	0.010	0.080	0.147	0.001	0.146
AA	O ₄ –H ₅	0.013	0.011	0.002	0.013	0.001	0.012
AA	O ₄ –H ₆	0.031	0.027	0.004	0.036	0.020	0.016
AA	O ₇ –H ₈	0.019	0.018	0.001	0.014	0.010	0.004
AA	O ₇ –H ₉	0.026	0.026	0.000	0.019	0.019	0.000
Book	O ₁ –H ₂	0.018	0.010	0.008	0.037	0.000	0.037
Book	O ₁ –H ₃	0.031	0.031	0.000	0.031	0.023	0.008
Book	O ₄ –H ₅	0.013	0.010	0.003	0.017	0.000	0.017
Book	O ₄ –H ₆	0.028	0.028	0.000	0.026	0.021	0.005

data in Table 1 indicate that penetration is significant in the AA water molecule, but is smaller or nonexistent elsewhere, including the “dangling” O–H bonds of the book isomer, which has a much smaller VEBE than the AA isomer. We have used these results to explain [152] the $\sim 300 \text{ cm}^{-1}$ O–H vibrational red-shifts that are observed experimentally in the infrared spectra of $(\text{H}_2\text{O})_n^-$ clusters that exhibit the AA binding motif [87,106,111,112,153]. This red shift is absent, or significantly smaller, in non-AA isomers. Curiously, this $e^- \rightarrow \sigma^*$ charge transfer appears to be an electron correlation effect; comparison of B3LYP and Hartree-Fock calculations reveals that the latter method predicts far less electron penetration into the water MOs, and also vibrational red-shifts that are far smaller than those observed experimentally. On the other hand, scaled harmonic frequency shifts computed at the B3LYP level are in reasonable agreement with experimental values, and the extent of charge transfer is markedly greater in the B3LYP calculations [152].

2.1.2. Many-electron calculation of the optical spectrum of $e^-(aq)$

The integrated oscillator strength measurement of Bartels and co-workers [145] unequivocally demonstrates that *excitations* of $e^-(aq)$ are not strictly one-electron transitions, while the various population analyses discussed in the previous section serve to indicate that H_2O frontier orbitals may support up to $\sim 20\%$ of the spin density in the ground state of hydrated-electron systems. It is important to recognize that these two types of “many-electron” character are not quite the same thing. The two effects can be separated in excited-state calculations based upon time-dependent (TD) DFT [154,155] which *does* incorporate many-electron character. At the same time, linear-response TD-DFT calculations rigorously satisfy a sum rule [154]

$$\sum_{n>0} f_{0 \rightarrow n} = 1, \quad (4)$$

meaning that TD-DFT excitations are strictly one-electron transitions. (Using a different kind of language, excitations of the unpaired electron within TD-DFT are quasi-particle excitations that are “dressed” by the polarization response of the solvent molecules.) In view of the aforementioned oscillator strength measurement [145], we therefore decided to undertake a TD-DFT calculation of the optical absorption spectrum of $e^-(aq)$ in bulk water, using a hybrid quantum mechanics/molecular mechanics (QM/MM) formalism to model the bulk liquid environment.

Although TD-DFT is probably the most widely-used method in excited-state quantum chemistry, it has become clear over the last few years that this approach, at least in conjunction with standard density functionals, is seriously flawed for large systems, especially liquids and clusters. In such systems, TD-DFT calculations are beset by a near-continuum of spurious, low-energy charge-transfer transitions [156–158] that are artificially stabilized (often by several electron volts) owing to the incorrect asymptotic decay of the exchange-correlation potential [159]. This problem afflicts essentially all contemporary density functionals, unless specific procedures are undertaken to correct the asymptotic behavior of the functional. In some cases, the envelope of the electronic absorption spectrum can still be recovered in a liquid simulation [158], nevertheless, these spurious states add considerable cost to the calculation, especially if more than a few excitation energies are desired.

We have recently shown [160–162] that these spurious states can be removed using “long-range corrected” (LRC) functionals [162–173]. LRC functionals employ a partition of the electron–electron Coulomb operator,

$$\frac{1}{r_{12}} = \frac{1 - \text{erf}(\mu r_{12})}{r_{12}} + \frac{\text{erf}(\mu r_{12})}{r_{12}}, \quad (5)$$

into a short-range contribution, $[1 - \text{erf}(\mu r_{12})]/r_{12}$, which decays to zero on a length scale of $\sim 1/\mu$, and a long-range background, $\text{erf}(\mu r_{12})/r_{12}$. The quantity μ is an adjustable parameter that controls the length scale of the range separation, and the basic idea is to utilize different theories at different length scales. The short-range part of the Coulomb operator is used in conjunction with standard density-functional exchange within the generalized gradient approximation (GGA), which provides a reasonably accurate account of short-range (dynamical) correlation. Full (*i.e.*, 100%) Hartree-Fock (HF) exchange is incorporated asymptotically, via the long-range part of the Coulomb operator, because HF exchange has the correct asymptotic distance dependence for a charge-separated state [159]. Consider an exchange-correlation functional of the form

$$E_{xc} = E_c + E_x^{\text{GGA}} + C_{\text{HF}} E_x^{\text{HF}}, \quad (6)$$

which might include some HF exchange, E_x^{HF} (if $C_{\text{HF}} \neq 0$), in addition to local GGA exchange, E_x^{GGA} . The LRC functional corresponding to Equation (6) is

$$E_{xc}^{\text{LRC}} = E_c + E_x^{\text{GGA,SR}} + C_{\text{HF}} E_x^{\text{HF,SR}} + E_x^{\text{HF,LR}}. \quad (7)$$

Our group has implemented a variety of short-range (SR) versions of local GGA exchange functionals [162,172] within the Q-Chem electronic structure package [174]. In this work, we utilize the LRC- μ BOP functional, which combines a short-range version of B88 exchange [175] that we call μ B88 [128], along with the “OP” correlation functional [176]. Recent work has shown that this functional, with $\mu = 0.33 a_0^{-1}$,⁴ is capable of

reproducing CCSD(T)-quality VEBEs for $(\text{H}_2\text{O})_n^-$ clusters [54,141]. This represents unprecedented accuracy for DFT VEBEs, which are usually much too large [44], and the accuracy results from elimination of self-interaction error associated with the SOMO. This orbital is largely localized away from the other MOs, and therefore benefits from the fact that LRC functionals are free of self-interaction for electrons separated by a distance $r \gg 1/\mu$. Some benchmark VEBE results are depicted in Figure 5(a). The B3LYP functional systematically overestimates the VEBEs, although calculations in larger clusters suggest that B3LYP errors are not always quite so systematic [44].

To calculate the bulk absorption spectrum of $e^-(aq)$ using TD-DFT, we first performed a molecular dynamics simulation of this species in bulk water at $T=300$ K, using a one-electron pseudopotential model developed by Turi and Borgis [49] that we believe provides a reasonable description of the structure of $e^-(aq)$ in bulk water [116]. (Details of the simulations can be found in Refs. [116] and [128].) From this simulation, we extracted more than 100 snapshots, separated by intervals of 0.5 ps. All water molecules within 5.5 Å of the centroid of the one-electron wavefunction were described using DFT (for a total of ≈ 28 water molecules, or about two full solvation shells). Additional water molecules were described using point charges from a force field. The resulting spectrum is shown in Figure 6(a), where we compare it to the experimental result. The calculated spectrum affords quite accurate values for both the location of the absorption maximum (1.72 eV) as well as the width of the Gaussian feature. At a qualitative level, these calculations also reproduce the tail that is observed on the high-energy side of the spectrum.⁵

Figure 6(b) shows some selected natural transition orbitals (NTOs) from the TD-DFT calculation. NTOs are obtained by diagonalizing the particle and hole parts of the difference density matrix (or, equivalently, by singular value decomposition of the transition density matrix) [177–179], and thus provide the best possible particle/hole description of a particular excited state. For the $e^-(aq)$ calculations presented here, a single particle/hole pair of NTOs typically accounts for >99.5% of the norm of the transition

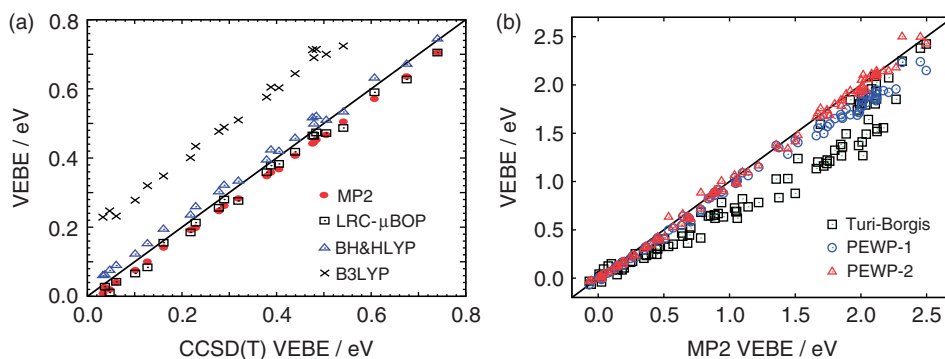


Figure 5 (colour online). Comparison of VEBEs for a database of $(\text{H}_2\text{O})_n^-$ isomers obtained from Ref. [140]: (a) various *ab initio* predictions, as compared to benchmark CCSD(T) results; and (b) predictions from several one-electron models, as compared to MP2 results. All *ab initio* calculations utilize the 6-31(1+,3+)G* basis set. [Panel (a) was adapted with permission from Ref. [54], incorporating some additional data here; copyright 2009 American Institute of Physics. Panel (b) was reprinted from Ref. [116]; copyright 2010 American Institute of Physics.]

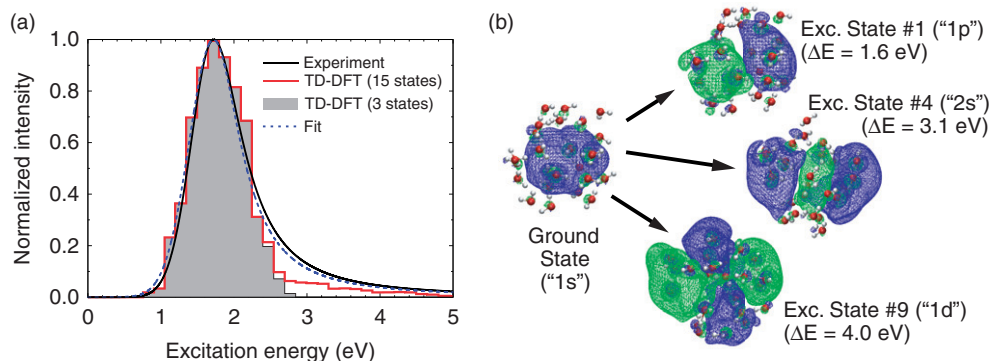


Figure 6 (colour online). (a) Electronic absorption spectrum for $e^-(aq)$ in bulk water, as computed using a QM/MM formalism in conjunction with the TD-LRC- μ BOP/6-31+G* level of theory ($\mu = 0.37a_0^{-1}$). Also shown are the experimental spectrum [93] and a fit of the TD-DFT data to the line shape function used in Ref. [93]. (b) Some selected natural transition orbitals (NTOs) from the TD-DFT calculation. The “ground state” (occupied) NTO is essentially identical for all of the excited states. (Adapted from Ref. [128]; copyright 2010 American Chemical Society.)

density matrix, hence the NTOs shown in Figure 6(b) provide an essentially exact depiction of the TD-DFT excited states.

Several important points can be gleaned from the NTOs shown in Figure 6(b). First, we note that the atom-centered Gaussian basis set that we employ (6-31+G*) is perfectly capable of describing the cavity-centered ground-state of the unpaired electron.⁶ Second, despite small contributions to these NTOs from oxygen $2p$ orbitals, the excitations shown in Figure 6 can be easily identified with eigenstates of the “particle in a spherical cavity” model.⁷ We interpret these TD-DFT results as evidence that the one-electron picture of $e^-(aq)$ spectroscopy is not fundamentally flawed.

2.2. Correlation and localization in clusters

As mentioned in Section 1, a debate continues to rage regarding the interpretation of $(\text{H}_2\text{O})_n^-$ cluster photo-electron data in terms of either surface-bound or cavity-bound states of the unpaired electron. Although both types of states can be identified in *ab initio* calculations [44,104,139,181,182] such calculations are too expensive to allow extensive conformational sampling. At the same time, simulations based on one-electron pseudopotentials reveal that the distribution of isomers is quite sensitive to the procedure that is used to prepare the ensemble [80]. This is perhaps unsurprising, given that the experimentally-observed isomer distribution is quite sensitive to nozzle temperature [84], and it means that extensive conformational sampling will be necessary in any simulations, in order to reach meaningful conclusions regarding the isomers that are probed in any experiment.

Fortunately, the correlation energy associated with the unpaired electron is fairly small, as discussed in Section 2.1, and one-electron pseudopotentials can profitably be brought to bear on hydrated-electron systems. At the same time, detailed investigation of electron correlation effects in surface- and cavity-bound isomers of $(\text{H}_2\text{O})_{20}^-$ and $(\text{H}_2\text{O})_{24}^-$

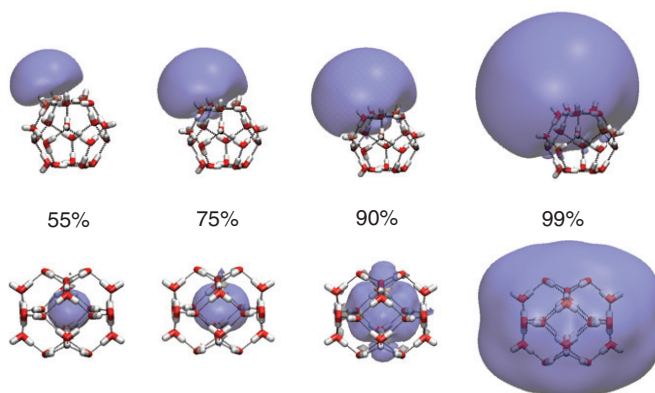


Figure 7 (colour online). Isoprobability surfaces encompassing different fractions of the Hartree-Fock SOMO, for a surface state of $(\text{H}_2\text{O})_{20}^-$ with a VEBE of 0.9 eV [MP2/6-31(1+,3+)G* level], and a cavity state of $(\text{H}_2\text{O})_{24}^-$ whose VEBE is 1.1 eV. At the resolution shown here, the very slight “orthogonalization tails” are not visible; see Ref. [140] for a version of this figure where both positive and negative lobes are visible. (Adapted from Ref. [140]; copyright 2008 American Chemical Society.)

clusters [140] reveals subtle differences that lead us to believe that a balanced description of the energetics for these two types of states will be difficult to achieve using a one-electron model, unless an accurate, polarizable water model is employed. These differences in electron correlation are the topic of this section.

Although the correlation energy associated with the unpaired electron is fairly small, as compared to that expected for valence electrons, Figure 4(b) reveals systematic differences in the value of Δ for surface states of $(\text{H}_2\text{O})_n^-$ clusters, as compared to cavity states. In particular, *all* of the surface-bound isomers that we have examined exhibit smaller values of Δ than *any* of the cavity-bound isomers. Because

$$\text{VEBE} = E_{\text{neutral}}^{\text{HF}} - E_{\text{anion}}^{\text{HF}} + \Delta, \quad (8)$$

a larger fraction of the VEBE arises from electron correlation in the case of cavity states than in the case of surface states.

It is also interesting to note in Figure 4(b) that the only data points that lie far from the best-fit line (for Δ versus VEBE) correspond precisely to the three *ab initio*-optimized cavity states included in the data set. These isomers correspond to geometries that were set up “by hand” (although subsequently optimized using DFT), by re-orienting some of the dangling hydrogen atoms in stable neutral clusters, with the intention of obtaining cavity states. We have no information about how the energies of these isomers compare to other local minima on the potential energy surface, and it is unlikely that they are low-energy isomers. Given that cavity-type isomers extracted from bulk $e^-(aq)$ simulations *do* lie close to the best-fit line, it seems likely that the *ab initio*-optimized cavity geometries are not representative of geometries that are sampled a liquid environment.

The larger value of Δ that is observed for cavity-bound isomers is a manifestation of the simple fact that a cavity-bound SOMO overlaps a larger number of water molecules, as

compared to a surface-bound SOMO. This is clearly evident from Figure 7, where we plot a series of isoprobability contours, encompassing ever-greater fractions of the SOMO, for two roughly-spherical $(\text{H}_2\text{O})_n^-$ isomers of comparable size and VEBE, but where one isomer exhibits a surface binding motif and the other is a cavity-bound state. In the former case, even an isosurface that encapsulates 99% of the probability density shows virtually no penetration into the interior of the cluster, whereas a 99% isoprobability contour for a cavity state of $(\text{H}_2\text{O})_{24}^-$ completely envelopes the cluster, which constitutes about two full solvation shells around the unpaired electron. The reason for this difference is that the main attractive part of the electron–water potential lies near the hydrogen atoms, and for a surface state, these hydrogen atoms are typically pointed outward in the vicinity of the SOMO, thereby facilitating surface binding. This leaves very little driving force for electron penetration into the cluster, where the oxygen lone pairs provide little in the way of an attractive potential. In the case of the cavity state, the main part of the SOMO localizes at the center of the clusters, where it is directly coordinated to several water molecules (four of them, for the particular isomer shown in Figure 7) that each have one hydrogen atom oriented toward the cavity. However, the orientation of the O–H bonds in the second solvation shell provides numerous regions where the electron–water potential is fairly attractive, thus facilitating delocalization of the SOMO throughout the second solvation shell.

A more quantitative analysis of the origins of Δ for surface versus cavity states can be obtained by decomposing the total electron correlation energy obtained at the MP2 level, $E_{\text{corr}}^{\text{MP2}}$, into a sum of pair correlation energies (PCEs) [140],

$$E_{\text{corr}}^{\text{MP2}} = \sum_{i < j}^{\text{occ}} E_{ij}^{\text{PCE}}, \quad (9)$$

each of which is given by

$$E_{ij}^{\text{PCE}} = \sum_{a < b}^{\text{virt}} \frac{|\langle \varphi_i \varphi_j | | \varphi_a \varphi_b \rangle|^2}{\varepsilon_i + \varepsilon_j - \varepsilon_a - \varepsilon_b}. \quad (10)$$

[We use standard notation for the Hartree-Fock occupied (i, j) and virtual (a, b) orbitals and energy levels.] Since the dispersion energy arises from fluctuations in two different charge distributions, induced by electron correlation, in the context of $(\text{H}_2\text{O})_n^-$ it makes sense to define the electron–water dispersion energy, $E_{e\text{-disp}}^{\text{MP2}}$, as the sum of all PCEs E_{ij}^{PCE} for which $j = \text{SOMO}$:

$$E_{e\text{-disp}}^{\text{MP2}} = \sum_{i \neq \text{SOMO}}^{\text{occ}} E_{i, \text{SOMO}}^{\text{PCE}}. \quad (11)$$

This definition of electron–water dispersion is equivalent to one proposed for dipole-bound anions by Gutowski and Skurski [183], who motivated this definition by means of a double perturbation expansion. For the surface-bound $(\text{H}_2\text{O})_{20}^-$ isomer shown in Figure 7, this analysis affords $E_{e\text{-disp}}^{\text{MP2}} = 0.27$ eV, which represents 30% of the total VEBE. For the cavity-bound state of $(\text{H}_2\text{O})_{24}^-$ that is shown in the same figure, we obtain $E_{e\text{-disp}}^{\text{MP2}} = 0.67$ eV, which amounts to 61% of the VEBE.

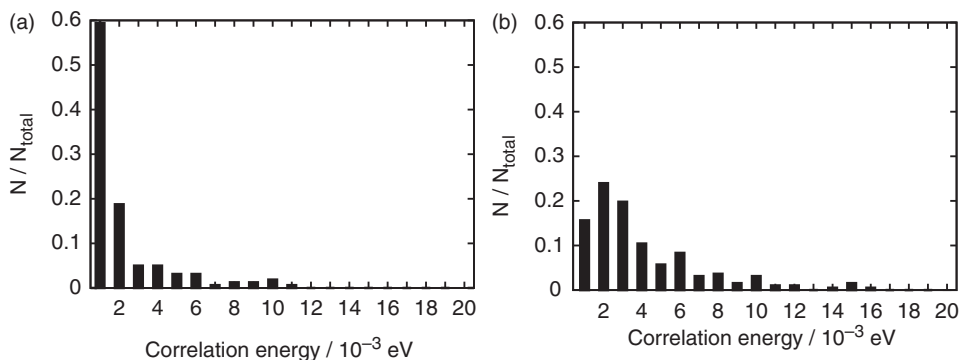


Figure 8. Histograms of MP2 SOMO pair correlation energies (SPCEs) for (a) the $(\text{H}_2\text{O})_{20}^-$ surface isomer from Figure 7 and (b) the $(\text{H}_2\text{O})_{24}^-$ cavity isomer from Figure 7. Both histograms are normalized, so what is plotted is the fraction of orbital pairs, N/N_{total} . The surface state in panel (a) shows a larger number of orbitals with a very small SPCEs, whereas the cavity state in panel (b) shows a large number of orbitals with moderate SPCEs. (Reprinted from Ref. [140]; copyright 2008 American Chemical Society.)

We have designated the quantities $E_{i,\text{SOMO}}^{\text{PCE}}$ in Equation (11) as SOMO pair correlation energies (SPCEs) [140]. To aid in interpreting these data, the SPCEs were computed in the basis of Boys-localized MOs [184]. In this basis, each doubly-occupied MO is mostly localized on a single H_2O molecule, while the SOMO is largely unaltered by the localization procedure [140]. The two isomers depicted in Figure 7 exhibit markedly different SPCE distributions, as shown in Figure 8. For the cavity-bound isomer, a much wider range of SPCEs is obtained, whereas in the surface-bound case, most of the SPCEs fall into the lowest-energy bin in Figure 8(a). These distributions are entirely consistent with the idea that the excess-electron wavefunction in a cavity-bound $(\text{H}_2\text{O})_n^-$ isomer overlaps (and therefore interacts strongly with) more water molecules than does the electron's wavefunction in a surface-bound isomer.

What is the significance of this observation for the development of one-electron pseudopotential models? When the electron's wavefunction envelops a water molecule, one may anticipate that the electrostatic environment of that molecule is quite different than it would be in the absence of the extra electron. In a surface-bound isomer of $(\text{H}_2\text{O})_n^-$, the electronic environment of most H_2O molecules is fairly similar to what it would be in a neutral cluster at the same geometry, whereas for a cavity-bound isomer, many (but not all) of the H_2O molecules experience an electrostatic environment quite different from neutral water. We expect that only a polarizable water model is capable of describing such differences, and we therefore suggest that a consistent treatment of the relative energetics and VEBEs for *both* surface- and cavity-bound $(\text{H}_2\text{O})_n^-$ cluster isomers demands a polarizable water model.

2.3. Shortcomings of simple water models

Differences in electron correlation energies as a function of binding motif might be considered a somewhat subtle feature of the electronic structure of $(\text{H}_2\text{O})_n^-$ isomers, but there exists far more dramatic evidence of the need for a polarizable water model.

According to various one-electron pseudopotentials, the electron–water interaction has a well depth of ~ 50 kcal/mol (≥ 2 eV) [49,116] and the incorporation of such an overwhelming interaction energy into a simple water force field can lead to dramatic divergences in certain regions of the $(\text{H}_2\text{O})_n^-$ potential energy surface, as we have documented previously [114]. Even if such divergent models provide a reasonable description of *certain* parts of the $(\text{H}_2\text{O})_n^-$ potential energy surface, the existence of unphysical divergences precludes the use of Monte Carlo sampling or other algorithms designed to explore global potential energy surfaces.

Even for models that do not fail so dramatically, there is a serious issue related to the relative accuracy with which the neutral and anionic potential surfaces are described. Oddly, this issue has not received much attention in the literature. The problem is illustrated in Figure 9(a), using cartoon potential energy surfaces for $(\text{H}_2\text{O})_n^-$ and $(\text{H}_2\text{O})_n$. Regardless of whether the anion is adiabatically bound or not (*i.e.*, whether the global minimum of $(\text{H}_2\text{O})_n$ lies below that of $(\text{H}_2\text{O})_n^-$), it is certainly true that there exist local minima on the $(\text{H}_2\text{O})_n^-$ potential surface for which the electron is bound in a vertical sense. One such local minimum is labeled “★” in Figure 9. Because the electron–water interaction energy is large and negative, the extra electron often has the effect of stabilizing water networks that would be extremely unfavorable in neutral water, hence the point labeled

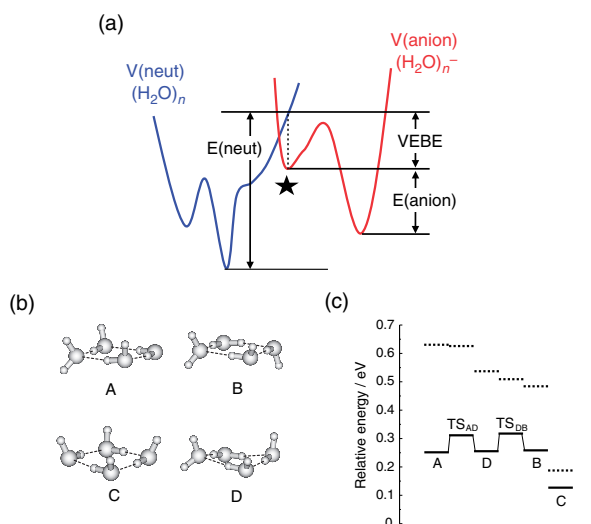


Figure 9 (colour online). (a) Schematic illustration of the potential energy surface of a $(\text{H}_2\text{O})_n^-$ cluster anion (shown in red) and the corresponding neutral cluster, $(\text{H}_2\text{O})_n$ (shown in blue), with various energetic quantities defined for the stable $(\text{H}_2\text{O})_n^-$ isomer labeled “★”. Both surfaces are plotted on a common energy scale, ergo this example represents a case where the anion “★” is *vertically* bound ($\text{VEBE} > 0$), but is *adiabatically* unbound since the $(\text{H}_2\text{O})_n$ global minimum lies below the $(\text{H}_2\text{O})_n^-$ global minimum. (b) Examples of stable isomers of $(\text{H}_2\text{O})_4^-$ that can be observed in the photo-electron spectrum of this cluster isomer [86], and subsequently assigned based on *ab initio* calculations [106,110] (c) Calculated energy levels for the $(\text{H}_2\text{O})_4$ and $(\text{H}_2\text{O})_4^-$ cluster isomers depicted in panel (b), along with some transition states; solid lines represent stationary points on the $(\text{H}_2\text{O})_4$ potential surface, and broken lines represent the $(\text{H}_2\text{O})_4^-$ cluster energy at the same geometry. The zero of energy in panel (c) corresponds to the $(\text{H}_2\text{O})_4$ global minimum, which is not shown. [Panels (b) and (c) are adapted from Ref. [114].]

“★” lies high above the global minimum on the $(\text{H}_2\text{O})_n$ potential surface. The electron–water interaction energy is generally much larger than typical water–water intermolecular interaction energies, and consequently the electron disrupts the native hydrogen bonding of neat liquid water.

A particular example of this phenomenon, for which accurate calculations are available, is the case $n = 4$. On the basis of *ab initio* calculations [106,110], the experimental photo-electron spectrum of $(\text{H}_2\text{O})_4^-$ has been assigned to four different cluster isomers, the structures of which are depicted in Figure 9(b). The main features in this spectrum arise from three quasi-degenerate $(\text{H}_2\text{O})_4^-$ isomers [110], which are labeled A, B, and D in Figure 9. Although these $(\text{H}_2\text{O})_4^-$ local minima are essentially iso-energetic, the neutral analogues of these three isomers are rather different in energy [110]. On the other hand, isomer C of $(\text{H}_2\text{O})_4^-$, which is similar in its structure to the global minimum of $(\text{H}_2\text{O})_4$ [185], is observed only as a weak, low-energy feature in the photo-electron spectrum [86], and the actual global minimum structure for $(\text{H}_2\text{O})_4$ does not bind an extra electron at all.

The above considerations indicate that removal of an electron from $(\text{H}_2\text{O})_n^-$ accesses high-energy regions of the $(\text{H}_2\text{O})_n$ potential energy surface, where minor changes in the geometry of the water network may alter the water–water energetics substantially. In this respect, the hydrated electron is certainly not unique; many other ions profoundly disrupt the hydrogen-bonding structure of neat liquid water, at least in the first solvation shell, thereby stabilizing water networks that would be highly unfavorable in the absence of the ion. The important difference here is that the VEBE is a key experimental handle for probing the structure of $(\text{H}_2\text{O})_n^-$. In contrast, in the case of $\text{I}^-(\text{H}_2\text{O})_n$ clusters (another system where, for a time, there was a surface-binding versus cavity-binding controversy [186]), one does not have the option of doing “halide ion ejection spectroscopy” to characterize structure. As such, theorists who wish to make contact with experiments on $\text{I}^-(\text{H}_2\text{O})_n$ are never faced with the difficult task of calculating the energy difference between $\text{I}^-(\text{H}_2\text{O})_n$ and $(\text{H}_2\text{O})_n$.

The upshot of these considerations is that calculation of VEBEs for $(\text{H}_2\text{O})_n^-$ clusters [and for bulk $e^-(aq)$ as well] is a rather demanding task, insofar as the magnitude of this quantity is often controlled more by the *neutral* water potential surface than it is by the $(\text{H}_2\text{O})_n^-$ potential surface [110,114,187], and in regions where the neutral structure is quite high in energy relative to its own global minimum. Because VEBEs are used to interrogate the structure of $(\text{H}_2\text{O})_n^-$ clusters, any plausible theory or model that attempts to make contact with these experiments must be capable of providing an accurate description of the *neutral* potential surface in these regions. Non-polarizable water models are simply not up to the task [54,116].

To illustrate these ideas, let us consider $(\text{H}_2\text{O})_{20}^-$, as described using the one-electron model of Turi and Borgis [49], which combines the “simple point charge” (SPC) water model [188,189] with an electron–water pseudopotential developed by Turi and Borgis. The Turi-Borgis hydrated-electron model has been widely used in recent simulations of both $(\text{H}_2\text{O})_n^-$ clusters and bulk $e^-(aq)$ [49,67,73–78]. Figure 10 shows a selection of the low-energy structures for $(\text{H}_2\text{O})_{20}^-$ that we were able to locate using the basin-hopping Monte Carlo method [190]. At $T = 150$ K (perhaps comparable to the temperature of a warm molecular beam), each of these isomers lies within a few $k_B T$ of the lowest-energy $(\text{H}_2\text{O})_{20}^-$ isomer. The corresponding $(\text{H}_2\text{O})_{20}$ isomer energies (*i.e.*, the values of the SPC water potential) vary widely and are quite high in energy, as compared to the putative

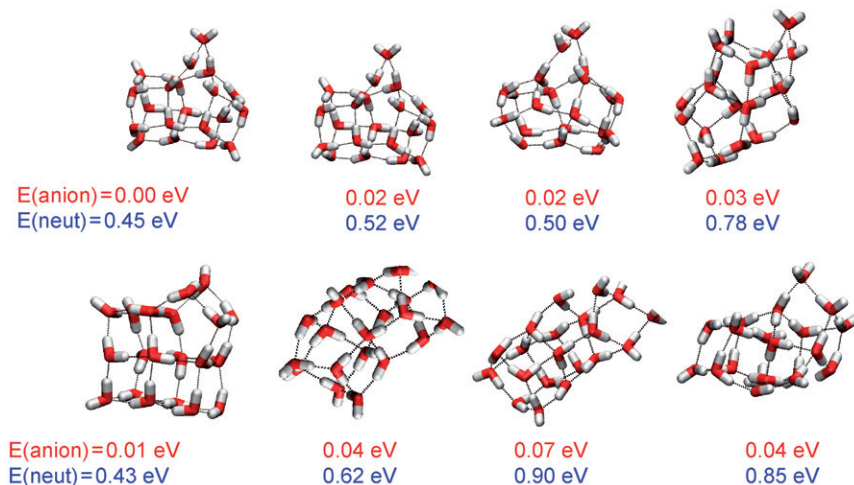


Figure 10 (colour online). Selected local minima on the $(\text{H}_2\text{O})_{20}^-$ potential surface, as described by a one-electron model potential [49]. (The excess-electron wavefunction is not shown, for clarity.) The energies of the anionic and neutral clusters are measured relative to the lowest-energy $(\text{H}_2\text{O})_{20}^-$ and $(\text{H}_2\text{O})_{20}$ structures that we were able to locate by means of extensive basin-hopping Monte Carlo searches; as such, these quantities correspond to the definitions introduced in Figure 9(a). Note that $k_B \times (150 \text{ K}) = 0.0125 \text{ eV}$.

global minimum for $(\text{H}_2\text{O})_{20}$ within the SPC model.⁸ [We take this minimum to define $E(\text{neut})=0$.] It is highly doubtful that the SPC water model is reliable for predicting the relative energies of cluster isomers that lie 0.5–1.0 eV (*i.e.*, up to 23 kcal/mol) above the neutral water global minimum. For smaller clusters ($n \leq 6$), we can confirm this suspicion using complete-basis MP2 calculations [54,116], as we will discuss in Section 3.2.

3. The delicate business of constructing a pseudopotential

As mentioned in the Introduction, many-electron *ab initio* methods are simply too expensive to provide the extensive configurational sampling that is necessary in order to study $(\text{H}_2\text{O})_n^-$ clusters. Although Car-Parrinello DFT simulations of both $(\text{H}_2\text{O})_n^-$ clusters and bulk $e^-(aq)$ have been reported [104,182,192], the exceedingly high cost of Hartree-Fock exchange in periodic calculations precludes the use of accurate LRC density functionals in such calculations. Given that many-electron contributions to the spectroscopy of these species appear to be small (albeit quantitatively important in some cases), we turn to one-electron models in which a single, unpaired electron is treated quantum-mechanically, via solution of the time-independent Schrödinger equation in a potential that is established by a water force field. Although this approach is sometimes termed “mixed quantum/classical molecular dynamics”, it is really nothing more than a QM/MM calculation that uses a one-electron QM region. As such, $\hat{H}\psi = E\psi$ can be solved—essentially exactly—on a three-dimensional, real-space grid. The unpaired electron (QM region) is adiabatically decoupled from the classical water molecules (MM region), and molecular dynamics for the water molecules is propagated using Hellmann-Feynman forces, $\partial E/\partial x = \langle \psi | \partial \hat{H} / \partial x | \psi \rangle$, on an adiabatic potential surface that corresponds to an

eigenvalue of \hat{H} . (In principle, this could be the potential surface corresponding to an excited state of the electron, although in this work we consider only ground-state dynamics.) We have developed efficient procedures for performing such simulations, for both polarizable and non-polarizable water models [54], including an efficient implementation of Ewald summation for bulk $e^-(aq)$ calculations [116].

Our chief aim in this section is to develop a one-electron model for the hydrated electron in which the underlying water model is accurate and polarizable. For this purpose we choose the AMOEBA water model [193–195], which employs atom-centered point charges, dipole moments, and quadrupole moments in order to describe the permanent electrostatics, and Thole-type atomic polarizabilities [196] to determine atom-centered inducible dipole moments. These dipole moments are determined self-consistently at each geometry [193]. This model provides good agreement with experimental data for the density, radial distribution function, enthalpy of vaporization, magnetic shielding, self-diffusion coefficient, and static dielectric constant of neat liquid water, across a broad range of thermodynamic conditions [194].

Having specified the model for the water–water interactions, the remaining ingredient is an electron–water interaction potential. Insofar as the water model contains electrostatic multipole moments, part of this interaction potential will consist of classical charge–multipole interactions. Other contributions to the potential have quantum-mechanical origins, including the electron–water exchange interaction and the Pauli repulsion energy, which arises from the requirement that the excess electron’s wavefunction must be orthogonal to the MOs on the water molecules. Early models of the solvated electron often employed simple, heuristic functional forms for these latter interactions, but such an approach is inconsistent with our goal of accurately describing the relative energies of different cluster isomers.

Starting with the work of Schnitker and Rossky [45], there have been several attempts to derive an interaction potential based on a rigorous (if approximate) quantum-mechanical description of H_2O^- . Interaction potentials derived in this way are really “pseudopotentials”, in the sense that they are scalar potentials, $V(\vec{r})$, for which the nodeless, ground-state eigenfunction of $\hat{T} + V$ is intended to reproduce the H_2O^- ground-state wavefunction (or more precisely, the singly-occupied MO) outside of the core molecular region. Two different procedures for deriving such a scalar potential are summarized in Section 3.1. Our own experience with these methods, leading to a polarizable electron–water pseudopotential (PEWP) model, are described in Section 3.2.

3.1. Some non-heuristic procedures

Most procedures that start from H_2O^- and arrive at an electron–water pseudopotential have, to date, been based upon the so-called static-exchange (SE) approximation [45,48,88,197] wherein one considers the interaction of an excess electron with the ground-state wavefunction of an isolated molecule, H_2O in the present case. The H_2O^- wavefunction, $|\Psi\rangle$, is taken to be an antisymmetrized product of the excess-electron orbital, $|\psi\rangle$, and the frozen MOs from a (neutral) H_2O calculation, $|\psi_i\rangle$. This leads to a one-electron eigenvalue equation for the excess electron [45,48,197]:

$$\hat{H}_{\text{SE}}|\Psi\rangle = (\hat{T} + V_n + V_H + \hat{V}_{xc})|\Psi\rangle = \varepsilon|\Psi\rangle. \quad (12)$$

Here, \hat{T} is the kinetic energy operator, V_n is the electron–nuclear interaction, V_H is the electronic Coulomb (Hartree) energy, and \hat{V}_{xc} is the (nonlocal) exchange–correlation operator. Historically, \hat{V}_{xc} has meant Hartree–Fock (HF) exchange only, and in fact this term is neglected entirely in the original treatment by Schnitker and Rossky [45]. It is also neglected by Wang and Jordan [50,136] in their development of the Drude–oscillator model for electron–water interactions. In our own work [116], which is described in Section 3.2, we will allow for both exchange and correlation, using a Kohn–Sham density–functional prescription. At any rate, the quantities V_H and \hat{V}_{xc} are identical to the Coulomb and exchange (or exchange–correlation) operators in a HF (or Kohn–Sham DFT) calculation of H₂O. As such, the highest occupied MO (HOMO) in the SE approximation is the lowest unoccupied MO (LUMO) in the HF or DFT calculation.

By assumption, the H₂O MOs used to construct $|\Psi\rangle$ are frozen, hence Equation (12) is a one–electron eigenvalue equation. Construction of $V_H + \hat{V}_{xc}$, however, requires an SCF calculation for H₂O, and this aspect must be removed in order to obtain a proper scalar potential, $V(\vec{r})$. Schnitker and Rossky [45] accomplished this by writing the SE wavefunction for the excess electron, $|\psi\rangle$, as a linear combination of the MOs from an isolated H₂O calculation along with a nodeless wavefunction, $|\phi\rangle$, that is asymptotically correct but lacks oscillations in the core molecular region:

$$|\psi\rangle = |\phi\rangle + \sum_i^{\text{occ}} c_i |\psi_i\rangle. \quad (13)$$

Inserting Equation (13) into Equation (12) affords an eigenvalue equation for the nodeless pseudo–wavefunction [45]:

$$\left(\hat{H}_{SE} + \sum_i^{\text{occ}} (\varepsilon - \varepsilon_i) |\psi_i\rangle \langle \psi_i| \right) |\phi\rangle = \varepsilon |\phi\rangle. \quad (14)$$

The second term in parentheses in Equation (14) is a repulsive potential that forces $|\phi\rangle$ to remain outside of the molecular region, thus preventing variational collapse.

The action of any operator, \hat{v} , on the ket $|\phi\rangle$ can be expressed in real space as an orbital–dependent scalar potential,

$$v[\phi](\vec{r}) = \frac{\langle \vec{r} | \hat{v} | \phi \rangle}{\phi(\vec{r})}. \quad (15)$$

As such, the repulsive potential in Equation (14) may be written as

$$V_{\text{rep}}(\vec{r}) = \sum_i^{\text{occ}} (\varepsilon - \varepsilon_i) \frac{\psi_i(\vec{r}) \langle \psi_i | \phi \rangle}{\phi(\vec{r})}. \quad (16)$$

Obviously, this potential depends on the nodeless pseudo–wavefunction itself, and to eliminate this dependence, Schnitker and Rossky make two subsequent approximations [45]: first, that the excess electron is weakly–bound ($|\varepsilon| \ll |\varepsilon_i|$); and second, that the nodeless function $\phi(\vec{r})$ is constant in the molecular region. The latter assumption is especially dubious, but without it, $|\phi\rangle$ is not uniquely defined by Equation (14), since the addition of any linear combination of the kets $|\psi_i\rangle$ also affords a solution to this equation [46,198].

In any case, the assumptions made by Schnitker and Rosicky lead to a very simple, analytic form for the repulsive potential [45]:

$$V_{\text{rep}}(\vec{r}) = - \sum_i^{\text{occ}} \varepsilon_i \psi_i(\vec{r}) \int d\vec{r}' \psi_i(\vec{r}'). \quad (17)$$

The integrals in this expression can be pre-computed in advance, and in practice the formula in Equation (17) is evaluated over a real-space grid and then fit to some analytic function.

The Schnitker-Rosicky repulsive potential has been used in numerous $e^-(aq)$ simulations [33–36], and a version of this procedure was employed to construct the repulsive potential used in the Drude model developed by Wang, Sommerfeld, and Jordan [50,51,136] which has been used in several studies of the structures and VEBEs for $(\text{H}_2\text{O})_n^-$ clusters [68–71]. However, recent work has pointed to errors in the original implementation of this procedure [55,199]. When these errors are corrected, the new potential is slightly more attractive near the oxygen atom, as compared to the original (erroneous) implementation, but is also significantly *less* attractive near the hydrogen atoms [55]. Wang and Jordan [136], in attempting to incorporate the Schnitker-Rosicky repulsive potential as part of their Drude model, find that this potential is too repulsive, so they scale it down by an unspecified *ad hoc* factor, in order to reproduce *ab initio* VEBEs. In later work by Sommerfeld and Jordan [51], the Schnitker-Rosicky procedure is reported to yield a repulsive potential that is too *attractive*, and consequently Sommerfeld and Jordan scale *up* the repulsive potential, by a factor of 6.8.

Recently, Smallwood *et al.* [46] have shown that the inherent indeterminacy surrounding the construction of $|\phi\rangle$ can be removed by supplying an additional constraint, thereby avoiding the assumption that $\phi(\vec{r})$ is constant in the molecular region. Given that $\phi(\vec{r})$ is supposed to be nodeless, Smallwood *et al.* choose the very reasonable constraint that $\langle \phi | \hat{T} | \phi \rangle / \langle \phi | \phi \rangle$ should be minimized. This requirement leads to an iterative recipe for calculating the nodeless pseudo-wavefunction [46]:

$$|\phi\rangle = |\psi\rangle + \sum_i^{\text{occ}} \frac{\langle \psi_i | \hat{T} | \phi \rangle}{\langle \phi | \hat{T} | \phi \rangle} |\psi_i\rangle. \quad (18)$$

Once $|\phi\rangle$ is determined by self-consistent iteration, the corresponding repulsive potential is constructed using Equation (15) and then fit to some analytic form for convenient evaluation.

Because the MOs used to construct the aforementioned potential are frozen, polarization is not included in this potential. Polarization is sometimes grafted onto the SE approximation, in the form of a two-body polarization potential of the form

$$V_{\text{pol}}(r) = - \frac{\alpha}{2(r^2 + C)^2}, \quad (19)$$

where α is the isotropic (spherically-averaged) polarizability of H_2O , and C is a constant [29,45,49,88]. (For a derivation of this functional form, starting from a model that includes many-body polarization, see Refs. [52] or [54].)

3.2. Our own efforts: PEWP-1 and PEWP-2

Our original aim was not to reinvent the electron–water pseudopotential, but rather to use one of the methods described above, but in conjunction with an accurate, polarizable water model, which in this work means the AMOEBA model [193,194]. In this way, we can include *many*-body polarization in the model, and we can treat both the water–water and the electron–water polarization interactions in a fully self-consistent manner. In particular, this means that the Schrödinger equation for the excess-electron wavefunction (whose Hamiltonian depends upon the water dipole moments) must be solved self-consistently along with the equation that determines the inducible AMOEBA dipoles, $\{\vec{\mu}_k^{\text{ind}}\}$. The latter equation is

$$\vec{\mu}_k^{\text{ind}} = \alpha_k \left(\vec{F}_k^{\text{MM}} + \vec{F}_k^{\text{QM}} \right), \quad (20)$$

where α_k is the isotropic polarizability of the k th MM site [193,196]. The electric field at the k th site includes a contribution \vec{F}_k^{MM} that arises from the other water molecules, and another contribution \vec{F}_k^{QM} that arises from the wavefunction.

Version 1.0 of our polarizable electron–water pseudopotential, or PEWP-1 [54], is described in Section 3.2.1 below. Despite promising results obtained for $(\text{H}_2\text{O})_n^-$ clusters, this approach proved to be a failure in bulk solution, which led us to take a somewhat different approach to developing the pseudopotential. The development of this new model, PEWP-2 [116], is discussed in Section 3.2.2.

3.2.1. PEWP-1: Success for clusters, failure for bulk $e^-(aq)$

Our original idea was simply to combine the Schnitker-Rosky repulsive potential, Equation (17), with the polarizable AMOEBA water model, neglecting exchange and correlation in order to be consistent with previous models based on this repulsive potential [45,50,51,68,136]. Comparison to the original Schnitker-Rosky model [45] might then afford insight into the role of many-body polarization. Because the water model is polarizable, it is necessary to fit damping parameters to attenuate the electron–water Coulomb interactions as $r \rightarrow 0$, in order to avoid a “polarization catastrophe” [196]. (Such parameters are also employed within the AMOEBA model itself [193].) Following the lead of Jordan and co-workers [51,136], we also fit an overall scaling factor for the repulsive potential in Equation (17). The scaling factor and Coulomb damping parameters were fit to reproduce *ab initio* VEBE benchmarks, and the result is the model that we term PEWP-1 [54].

The performance of PEWP-1 for VEBE benchmarks is shown in Figure 5(b), which also depicts results obtained using the one-electron model developed by Turi and Borgis (hereafter, TB) [49]. The TB model does not utilize the Schnitker-Rosky form of the repulsive potential, but instead introduces a flexible, nine-parameter functional form for V_{rep} , which is then fit in order to reproduce the ground-state energy $[\varepsilon$ in Equation (12)] and density $(|\phi(\vec{r})|^2)$ of the SE pseudo-wavefunction. Consistent with other non-polarizable models discussed above, the TB model neglects \hat{V}_{xc} , utilizes an *ad hoc* electron–water polarization potential of the form given in Equation (19), and is coupled to the SPC water model [188,189]. The TB model has been used in many recent simulations of both water cluster anions and bulk $e^-(aq)$ [49,67,73–78] including a controversial [200,201] recent paper concerning the identity of $(\text{H}_2\text{O})_n^-$ isomers observed in photo-electron

experiments [73]. Owing to its central role in the theoretical description of hydrated-electron systems, the TB model serves as a useful baseline against which we will assess the accuracy of polarizable models.

Figure 5(b) shows that the PEWP-1 model is indeed more accurate than the TB model for VEBE benchmarks, especially at higher binding energies. Admittedly, in developing PEWP-1 we used this same VEBE database in order to fit a small number of Coulomb damping parameters. However, in Ref. [54] we also demonstrated that PEWP-1 is far more accurate for reproducing the relative energies of different $(\text{H}_2\text{O})_n^-$ and $(\text{H}_2\text{O})_n$ cluster isomers, affording relative isomer energies that are within ~ 1 kcal/mol of complete-basis MP2 results [54], even for neutral isomers that are rather high in energy. This is primarily attributable to the fact that the AMOEBA water model that underlies PEWP-1 is far more accurate for predicting the relative energetics of neutral $(\text{H}_2\text{O})_n$ clusters than is the SPC water model.

At the time that we developed PEWP-1, we had not yet implemented periodic boundary conditions within our simulation code, so only finite cluster benchmarks were reported [54]. Subsequently, we did extend these simulations to the bulk, with bizarre and unexpected results. In bulk solution, the PEWP-1 model fails to localize the electron into a cavity, in contrast to nearly every other one-electron model that has been developed over the past 25 years.

A good example of a cavity-type wavefunction can be seen in Figure 1(c). The cavity-centered SOMO in clusters such as this is stable with respect to geometry optimization [44,139] and remains localized in the cavity.⁹ Plane-wave DFT calculations of $e^-(aq)$ in bulk water also exhibit a cavity-bound SOMO that is stable with respect to room-temperature molecular dynamics [192]. In addition, there is also compelling experimental evidence for electron localization in polar fluids [123,124,202].

In contrast, the PEWP-1 model affords more delocalized $e^-(aq)$ wavefunctions, examples of which are shown in Figure 11. In these snapshots, one sees little evidence that the H_2O molecules re-orient to coordinate to the electron, and little evidence of solvation shell structure. Both observations are consistent with the largely structureless radial distribution functions (RDFs) that we obtain using this model, which are shown in Figure 12(a). Both the electron–hydrogen and the electron–oxygen radial distribution functions, $g(r)$, exhibit significant amplitude for $r < 1 \text{ \AA}$, meaning that the electron penetrates deep into the core molecular region, despite the presence of a (scaled) repulsive potential of the Schnitker-Rosky type. Shell structure *is* observed in models that predict cavity formation, as shown for example in the RDFs of Figure 12(b), which are obtained from a cavity-forming model that we will introduce in Section 3.2.2. The RDFs in

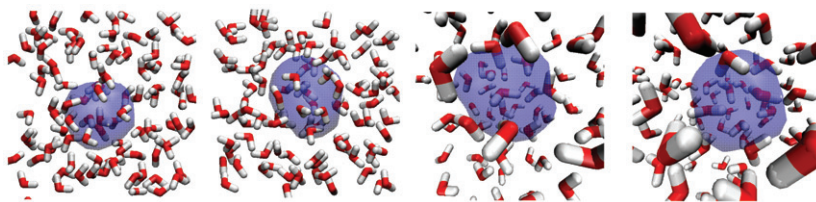


Figure 11 (colour online). Isoprobability surfaces encapsulating 90% of the PEWP-1 wavefunction for $e^-(aq)$.

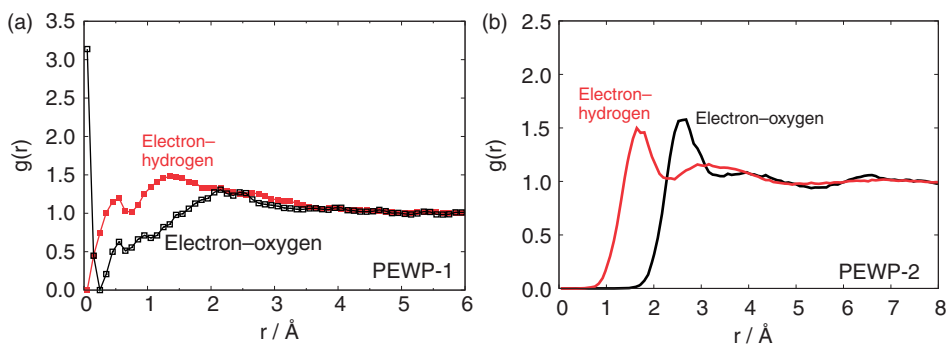


Figure 12 (colour online). Radial distribution functions, $g(r)$, for $e^-(aq)$ in bulk water, obtained from (a) the PEWP-1 model and (b) the PEWP-2 model. The origin of the coordinate r is the centroid of the electron's wavefunction. [Panel (b) is reprinted from Ref. [116]; copyright 2010 American Institute of Physics.]

Figure 12(b) are qualitatively similar to those obtained using other cavity-forming models, and although the peaks in $g(r)$ are broad, relative to what is obtained for classical anions such as Br^- or I^- , they are nonetheless well-defined, unlike what we obtain using PEWP-1.

Adding to these concerns is that fact that the diffusion coefficient that we calculate for the PEWP-1 model of $e^-(aq)$ is much too large. At $T = 300$ K, we obtain $D \gtrsim 1.0 \text{ \AA}^2/\text{ps}$, as compared to an experimental value of $D = 0.51 \text{ \AA}^2/\text{ps}$ at the same temperature [203]. The non-polarizable Turi-Borgis model [49], which does localize the electron into a cavity, predicts a much more reasonable value, $D = 0.6 \text{ \AA}^2/\text{ps}$ [67]. Note that $e^-(aq)$ diffusion is extremely rapid; with the exception of $\text{H}^+(aq)$ and $\text{OH}^-(aq)$, both of which are “special” in the sense that they have available a Grotthuss-type diffusion mechanism [204,205] the aqueous electron is the fastest species in water, with an ion mobility almost three times larger than that of $\text{K}^+(aq)$ [122]. Simulations of $e^-(aq)$ diffusion, using two different cavity-forming model potentials [47,67] have concluded that $e^-(aq)$ diffusion occurs via librational motions of the water molecules, the same motions that facilitate Grotthuss-type diffusion of OH^- in water [205]. This may explain why the ion mobility of $e^-(aq)$ is quite similar to that of $\text{OH}^-(aq)$ [122]. In cavity-forming $e^-(aq)$ models, these librational motions (which cause transient dissolution of water–water hydrogen bonds) serve to open up an empty solvent cavity, and at the same time may squeeze the electron out of the cavity that it presently occupies.

That we obtain a diffusion coefficient that is too large by (at least) a factor of two would be easier to forgive were the diffusion not so fast. The AMOEBA water model that we employ recovers the correct temperature- and pressure-dependence for various properties of water, and predicts an accurate value for water's self-diffusion coefficient [194]. Therefore it is difficult to imagine that any spurious water fluctuations, except possibly those induced by a qualitatively incorrect electron–water potential, could be responsible for the anomalously large value of D that we obtain for $e^-(aq)$. In our PEWP-2 simulations, we observe that the electronic wavefunction simply barrels through the liquid, without the need to wait for a new cavity to open up.

In our view, these bulk results indicate that the PEWP-1 electron–water potential is insufficiently repulsive. Evidently, however, attenuation of the electron–multipole

Coulomb operators can compensate for dramatic scaling of the repulsive potential, at least when it comes to reproducing VEBE benchmarks for clusters. If we avoid scaling down the Schnitker-Rosky repulsive potential, however, we find that we are unable to reproduce VEBE benchmarks within our target accuracy of ~ 0.1 eV. Nevertheless, the failure of PEWP-1 to localize the electron in bulk water, and the excessively large diffusion coefficient that this model predicts for $e^-(aq)$, serve as evidence that the repulsive potential has been reduced too much.

3.2.2. PEWP-2: A new approach

In view of the apparent failure of the PEWP-1 model in bulk solution, we decided to revisit the parameterization of the electron–water pseudopotential. Evidently, fitting the electron–water potential to reproduce *ab initio* benchmarks can mask serious problems with the bulk behavior, and it would be preferable to have an entirely first-principles algorithm to determine the interaction potential. In principle, the automated prescription of Smallwood *et al.* [46] offers such a prescription, as discussed in Section 3.1. To summarize, Equation (18) is used to determine a nodeless pseudo-wavefunction, based on Hartree-Fock calculations for H_2O^- , and subsequently Equation (15) is used to determine a (scalar) repulsive potential, $V_{\text{rep}}(\vec{r})$. (Actually, this procedure is not quite as well-defined as it sounds, since H_2O^- is not a bound species at the Hartree-Fock level, hence the excess electron must be confined in some artificial way [49,56].)

Our attempts to develop a useful interaction potential based on this procedure were unsuccessful, as the resulting potential is far too repulsive in the core molecular region. In our view, this approach affords a potential that is much too repulsive for use in conjunction with damped electrostatics, which attenuate the attractive interactions at short range. This explains why, in developing PEWP-1, it was necessary to scale down the Schnitker-Rosky repulsive potential. Ultimately, we were not able to construct from the Smallwood procedure any pseudopotential model that was accurate for cluster VEBE benchmarks but would also localize the electron and afford a reasonable diffusion coefficient.

Recently, Larsen *et al.* [56] reported a one-electron model built upon the pseudopotential construction procedure of Smallwood *et al.* [46], in conjunction with the non-polarizable SPC water model. In bulk water, this model does not localize the electron to nearly the same extent as previous models, and in fact affords $e^-(aq)$ wavefunctions that look a lot like the PEWP-1 wavefunctions in Figure 11. Larsen *et al.* [56] explain that this delocalization arises, at least in part, due to the existence of a shallow attractive potential well near the oxygen atom, which is absent in other pseudopotentials. The existence of such a feature, however, seems inconsistent with the surface-bound HF SOMOs that are depicted in Figure 7. The pseudopotential of Larsen *et al.* is supposed to approximate the all-electron HF result, but if indeed the orbital-dependent HF potential for the SOMO were attractive near the oxygen atom, then one would expect that these SOMOs would exhibit some penetration into the interior of the cluster. We observe no such penetration, even when a 99% isoprobability contour is used to plot the SOMO.

The diffusion coefficient of $e^-(aq)$ was not reported in Ref. [56], but our own preliminary calculations suggest that it is considerably larger than the experimental value at $T = 300$ K. Moreover, VEBEs predicted by this model are much less accurate, and the

errors far less systematic, than those obtained using the TB model, which also uses the SPC water model [116]. Further evaluation is needed before this model can be rejected outright, but preliminary results suggest that it suffers from many of the same problems that we encountered in our own attempts to use the automated procedure of Smallwood *et al.* [46]. It is not clear to us whether these features are inherent to the SE approximation itself, or whether they are artifacts of fitting the scalar potential to an analytic functional form. This question certainly warrants further investigation.

Instead, after considerable experimentation, we arrived at the procedure that is described below [116]. While not completely first-principles in nature, this approach has some intuitive physical appeal and—importantly—is fit to reproduce features of the SE wavefunction *but is not directly fit to reproduce any calculated or measured observables*. Unlike previous SE treatments, we will use LRC-DFT to obtain an electron–water exchange-correlation potential. We first solve Equation (18) for the nodeless pseudo-wavefunction, $|\phi\rangle$, using water MOs from a LRC- μ BOP calculation. Once a self-consistent solution has been determined, we construct a scalar potential for exchange via Equation (15) with $\hat{v} = \hat{V}_{xc}$.

To this exchange-correlation potential we must add a repulsive potential to replace the orbital orthogonality requirement. We fit this repulsive potential, along with damping parameters for the Coulomb interactions between the electron and the permanent AMOEBA multipoles, in order to reproduce the density maximum of the LUMO near the core molecular region. The repulsive potential is fit using the same functional form used previously by Turi and Borgis [49] to obtain a scalar potential that reproduces the SE pseudo-wavefunction. Following those authors, we apply a confining potential to maintain the excess electron near the core region. Lastly, we require damping parameters for the Coulomb interactions between the electron and the inducible water dipoles. We see no *a priori* reason why these damping parameters should be the same as those employed for the permanent electrostatic interactions, and damping parameters for the electron/inducible dipole interactions were fit to reproduce an electron–water polarization potential computed at the MP2 level [116].

We do not directly fit to any VEBEs or other observables *per se*, but we do reject any fits that do not reproduce *ab initio* VEBEs to within ~ 0.1 eV. Additional details regarding the SE calculations and the fitting procedure can be found in Ref. [116]. In the end, the interaction potential that we obtain is fairly similar to the one obtained by Turi and Borgis [49], and direct comparisons between the two can be found in Ref. [116]. The important difference is that our potential is carefully parameterized for use with a high-quality water model, and is specifically designed to allow for a self-consistent treatment of many-body polarization. The effect of these differences is immediately clear in the calculation of cluster VEBEs, which are depicted in Figure 5(b). Not only does the PEWP-2 model significantly outperform the TB model for these benchmarks, but in fact it outperforms PEWP-1 as well, even though the latter was specifically parameterized using this database of benchmark VEBEs. Statistical summaries of the errors in PEWP-2 VEBEs (Table 2) show that we have achieved our goal of ~ 0.1 eV accuracy in VEBEs.

Good performance for clusters is necessary but not sufficient to demonstrate the adequacy of a pseudopotential model; we also want to be able to describe the bulk species using the same model. In bulk water, the PEWP-2 model does localize the wavefunction in a cavity, and reasonably accurate values are obtained for other known properties of

Table 2. Mean unsigned errors (MUE) and maximum absolute deviations (MAD) for various one-electron models, relative to MP2/6-31(1+.3+)G* benchmarks for the database of VEBE benchmarks depicted in Figure 5(b). (Adapted from Ref. [116]; copyright 2010 American Institute of Physics.)

One-electron model	MUE/eV	MAD/eV
TB	0.253	-0.746
PEWP-1	0.105	-0.348
PEWP-2	0.041	0.184
LRC- μ BOP	0.037	0.224

Table 3. Properties of $e^-(aq)$ as predicted by our PEWP-2 model and the non-polarizable Turi-Borgis (TB) model [49], in comparison to experimental results. Except where indicated, all values correspond to $T = 300$ K.

Property	Experiment	One-electron model	
		PEWP-2	TB
VEBE/eV	3.3–4.0 ^a	3.7	4.8
Radius of gyration/Å	2.45 ^b	2.25	2.42
Optical absorption maximum/eV	1.72 ^c	1.75	1.92
Diffusion coefficient/Å ² ps ⁻¹	0.51 ^d	0.79 ± 0.16 ^e	≈0.6 ^f

^aRange of values that includes two cluster extrapolations [93,99] and several liquid jet experiments [96–98].

^bFrom moment analysis of the absorption spectrum [101].

^cBased on line-shape analysis of experimental data [93].

^dFrom Ref. [203].

^eUncertainties represent a 95% confidence interval averaged over four trajectories in simulation cell containing 100 H₂O molecules.

^fFrom Ref. [67], at $T = 298$ K.

the bulk species, as shown in Table 3. Notably, this includes the diffusion coefficient, which remains a bit too large, although considering the error bars it is not too much larger than that obtained using the TB model, which is also a bit too large. The radius of gyration,

$$r_g = \left\langle |\vec{r} - \langle \vec{r} \rangle|^2 \right\rangle^{1/2}, \quad (21)$$

is about 10% smaller than that inferred based on moment analysis of the experimental absorption spectrum [101], but the absorption maximum is in quantitative agreement with experiment. Prior to this work, the TB model was the most accurate one-electron model in this respect; other pseudopotential models predict absorption maxima that are even further to the blue [49].

4. The role of polarization in the bulk species, $e^-(aq)$

Equipped now with a polarizable, one-electron pseudopotential model for the hydrated electron, which appears to achieve near-quantitative accuracy for $(\text{H}_2\text{O})_n^-$ clusters, and which agrees qualitatively or semi-quantitatively with several known experimental properties of bulk $e^-(aq)$, we are set to ask: what is the importance of polarization in these systems, according to this model? This question is answered below.

We should emphasize that our PEWP-2 model, and the calculations presented below and in Refs. [116] and [128], represent the first time that a *carefully-parameterized, polarizable* hydrated electron model has been brought to bear on the bulk species, $e^-(aq)$.¹⁰ Although the Drude model of Jordan and co-workers has been developed for use with a polarizable water model [50–52], the Drude model is quite expensive and to date has not been implemented using periodic boundary conditions. (In fact, analytic energy gradients for the Drude model have been implemented only recently [142].)

The results presented in this section were obtained from ground-state molecular dynamics simulations using periodic unit cells ranging in size from 100–600 water molecules. Importantly, we utilize Ewald summation for the long-range electrostatic interactions, as cruder approximations such as the minimum-image convention afford ~ 1 eV errors in bulk VEBEs [78]. For technical details, the reader is directed to Ref. [116].

On a side note, our analysis of the PEWP-2 model for $e^-(aq)$ in bulk water [116] shows several interesting structural features that have not been pointed out in previous simulations. For example, analysis of the number of hydrogen bonds per water molecule, as a function of the distance from the centroid of the $e^-(aq)$ wavefunction, shows a significant disruption of the hydrogen-bonding network in the first *two* solvation shells, with recovery of bulk-like hydrogen bonding by the third solvation shell. [Recall that the 95% isoprobability contour for the cavity-like state in Figure 1(c) envelopes two full solvation shells.] We also find that H_2O molecules in the first two solvation shells undergo amplified librational dynamics, relative to what is observed in bulk liquid water, with the bulk limit once again recovered in the third solvation shell. These observations are consistent with the idea that water molecules nearby the electron are poor H-bond donors, on account of the diffuse nature of the ion, which provides little restoring force for librational perturbations. This is precisely the picture that has been inferred based upon resonance Raman spectra of $e^-(aq)$ in isotopically-substituted bulk water [113]. A fluxional solvation environment around the electron is also consistent with the large, positive value of $\Delta S_{\text{hyd}}^\circ$ [125,126].

The aforementioned structural features do *not* appear to be manifestations of polarization, as we observe them also in simulations using the non-polarizable TB model [116]. Since this review is focused on polarization, we shall not discuss these structural features any further. The interested reader is directed to Ref. [116].

4.1. Vertical electron binding energy

We calculate the bulk VEBE by averaging over several molecular dynamics runs, in various simulation cells, then extrapolating to the infinite-dilution limit; these extrapolations are depicted in Figure 13. For the non-polarizable TB model, the VEBE is (up to a sign) simply the ground-state electronic energy, and extrapolates to a value of 4.79 ± 0.09 eV at infinite dilution. (Uncertainties reported here represent a 95% confidence

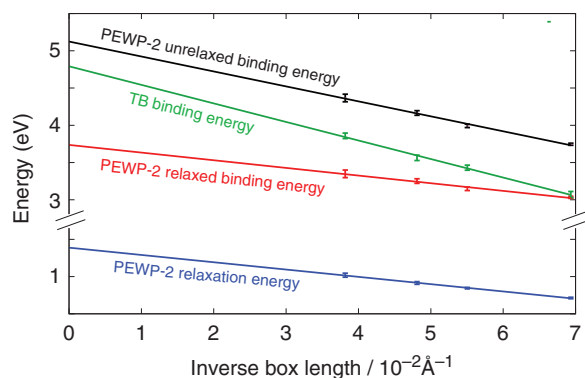


Figure 13 (colour online). Extrapolation of the VEBE for bulk $e^-(aq)$, as a function of inverse simulation cell length. (Reprinted from Ref. [116]; copyright 2010 American Institute of Physics.)

interval.) This is considerably larger than all previous reports of the bulk VEBE using the TB model, which include a value of 3.12 eV calculated using the minimum-image convention [49], a value of 3.9 eV determined using Ewald summation (with an unspecified simulation cell size) [78], and a value of 4.4 eV determined by extrapolating cluster VEBEs [78]. That our Ewald-summed value is so much larger than what is reported in Ref. [78] is not altogether surprising, given the sensitivity of the VEBE to the size of the simulation cell (see Figure 13), but it is intriguing that our infinite-dilution value is 0.3–0.4 eV larger than that reported based on cluster extrapolation.

Figure 13 also shows three separate extrapolations for the PEWP-2 model: a “relaxed” binding energy, an “unrelaxed” binding energy, and the difference between the two, which we call the relaxation energy. (Relaxation here refers to the response of the H_2O inducible dipoles to removal of the electron, *i.e.*, electronic re-organization at fixed nuclear coordinates.) The slope and intercept of the unrelaxed binding energy extrapolation are similar to those obtained for the TB model, where no relaxation is possible, which makes sense because the dielectric constant of the two systems should be quite similar. However, the relaxed binding energy in our model extrapolates to a much smaller value, 3.70 ± 0.07 eV.

The PEWP-2 prediction for the bulk VEBE lies between the value of 4.0 eV obtained by extrapolating photo-electron data for cold $(\text{H}_2\text{O})_n^-$ clusters collected in an ion trap [99] (which may or may not be reasonable analogues of a room-temperature liquid) and the value of 3.4 ± 0.2 eV obtained [93] by extrapolating older photo-electron data for warmer clusters [82]. However, the latter data extend only to $n = 69$, whereas newer data [84] extend to $n = 200$. As pointed out recently [97], the error bars on the extrapolation probably increase in light of the new data, and it appears as if an extrapolation using all existing data in the “Isomer I” series (Figure 2) would afford a VEBE greater than 3.4 eV. Very recently, three different groups have reported direct measurements of the bulk VEBE, using liquid microjets; the VEBEs reported in these experiments are 3.27 ± 0.10 eV [96], 3.3 eV [97], and 3.6 ± 0.1 eV [98]. It is unclear to us which of these measurements is most reliable, but the weight of all available evidence seems to be steering the bulk VEBE toward a value that is certainly no smaller—and possibly a bit larger—than the value of 3.4 eV extrapolated by Coe *et al.* [93] As such, our PEWP-2 value of 3.7 eV is not unreasonable.

Let us now consider the physics behind this number. The atom-centered inducible dipoles in our model represent electronic degrees of freedom, albeit coarse-grained ones, and should therefore remain in equilibrium with the QM electron, relaxing on the same time scale as electronic excitation or electron detachment. We see from Figure 13 that the relaxation energy extrapolates to a surprisingly large value, 1.37 ± 0.04 eV, which reveals a very important fact about non-polarizable solvated-electron models. Specifically, it explains why the non-polarizable TB model can be systematically *underbinding* in small clusters [as seen in Figure 5(b)], yet *overbinding* in the bulk limit. The explanation is simply that the solvent electronic degrees of freedom cannot relax following electron detachment, within the TB model. While the magnitude of this correction is quite large, at least in the bulk, this does not imply that the non-polarizable models are inherently flawed for all properties. The relaxation energy does not affect the ground-state forces, so ground-state structure and dynamics may be largely insensitive to the lack of polarization, and indeed, the structural properties predicted by PEWP-2 are fairly similar to those obtained using the TB model [116]. At the same time, it is clear that some correction needs to be applied to binding energies calculated using non-polarizable models, especially in the bulk limit. We expect this to be the case in any polarizable medium, not just water.

To summarize, we are attributing 1.4 eV of our 3.7 eV binding energy to electronic re-organization (*i.e.*, solvent polarization) following vertical electron detachment. To cross-check this value, we employ a Born-like dielectric continuum model for ion solvation, originally developed by Makov and Nitzan [207], which uses the optical (infinite-frequency) dielectric constant, ϵ_∞ , to model electronic relaxation. A non-polarizable solvent model corresponds to $\epsilon_\infty = 1$, whereas water's actual optical dielectric constant is 1.8. We will use the difference between VEBEs obtained for $\epsilon_\infty = 1.0$ versus $\epsilon_\infty = 1.8$ as a continuum approximation for the electronic re-organization energy.

In addition to ϵ_∞ and the static dielectric constant ($\epsilon = 78$), the input parameters to the Makov-Nitzan model are the mean electronic kinetic energy, $\langle \hat{T} \rangle$, and a cavity radius for the ion, which we take to be the electron's radius of gyration, r_g [Equation (21)]. Taking these parameters from bulk simulations, the continuum model predicts a relaxation energy of 1.3 eV for the TB model and 1.4 eV for PEWP-2 (see Table 4), in excellent agreement with the value extrapolated from simulations with explicit many-body polarization (see Figure 13). Furthermore, if we subtract 1.3 eV from the TB binding energy in the infinite-dilution limit, we obtain a corrected VEBE of 3.5 eV, in reasonable agreement with the

Table 4. Input parameters and results from application of the Makov-Nitzan dielectric continuum model. (Reprinted from Ref. [116]; copyright 2010 American Institute of Physics.)

Property	One-electron model	
	TB	PEWP-2
$r_g/\text{\AA}$	2.45	2.25
$\langle \hat{T} \rangle/\text{eV}$	1.6	1.7
VEBE($\epsilon_\infty = 1.0$)/eV	4.2	4.6
VEBE($\epsilon_\infty = 1.8$)/eV	2.9	3.2
Relaxation energy/eV	1.3	1.4

value of 3.70 ± 0.07 eV obtained from PEWP-2 simulations, especially in view of the fact that cluster benchmarks indicate that the TB model is underbinding, relative to PEWP-2, by ~ 0.25 eV. We take these results as confirmation that electronic re-organization of the solvent reduces the VEBE by ~ 1.4 eV in bulk water.

4.2. Excited electronic states

Electronic excitation energies are another property where one might anticipate large polarization effects. From a phenomenological point of view, excited-state calculations within the PEWP-2 model should involve converging the solvent dipoles self-consistently with the *excited-state* wavefunction. One problem with the implementation of such an approach is that the dipoles become state-specific, and therefore the Hamiltonian, $\hat{H} = \hat{H}[\{\mu_i\}]$, is state-specific as well. This means that the various excited-state wavefunctions need not be mutually orthogonal, since they are eigenfunctions of different Hamiltonians. Actually, this is a general problem for excited-state QM/MM methods based on polarizable MM force fields, a topic of considerable recent interest [208–213], and the same issue arises in all-electron calculations based upon the “maximum overlap method” [214]. The latter has recently been used to locate excited-state solutions to the SCF equations [161,214,215] or in other words, MO-based excited-state wavefunctions that include orbital relaxation in the excited state.

A second problem, which may be more specific to this particular chemical system, is that the electronic re-organization energy is quite large (~ 1 eV) in comparison to the typical spacing between excited-state energy levels (~ 0.1 eV). In practice, we are unable to converge the dipoles and the excited-state wavefunctions self-consistently, owing to problems associated with state-switching.¹¹ Inspired by the aforementioned maximum overlap method, we implemented a procedure wherein initial guesses for the excited-state wavefunctions are computed in the field of the ground-state dipoles, and then a maximum-overlap criterion is used to select the appropriate electronic state as the Hamiltonian is iteratively diagonalized, with solvent dipoles that are converged to the electronic state of interest. We found that this procedure was incapable of converging more than a few excited states, so an alternative was sought.

Perturbation theory offers a simple and straightforward way to incorporate dipole relaxation. We define a state-specific perturbation [116,128]

$$\hat{W}_n = \hat{H}[\{\mu_i^{(n)}\}] - \hat{H}[\{\mu_i^{(0)}\}], \quad (22)$$

where $\{\mu_i^{(0)}\}$ represents the set of dipoles converged to the ground-state wavefunction, whereas $\{\mu_i^{(n)}\}$ is the set of dipoles converged to the n th excited-state eigenfunction of the ground-state Hamiltonian, $\hat{H}[\{\mu_i^{(0)}\}]$. Because the perturbation is state-specific, each “relaxed” (*i.e.*, perturbed) excited-state wavefunction is an eigenfunction of a *different* Hamiltonian, and therefore the various excited states need not be mutually orthogonal. Among other consequences, this implies that the Thomas-Reiche-Kuhn sum rule [Equation (3)] need not be satisfied, and that transition dipoles depend upon the choice of coordinate origin. To mitigate these problems, we do not allow the excited-state wavefunctions to mix with the ground state in the perturbative correction to the zeroth-order states, which at least ensures that $\langle \psi_0 | \psi_n \rangle = 0$. As a result, the transition dipoles are

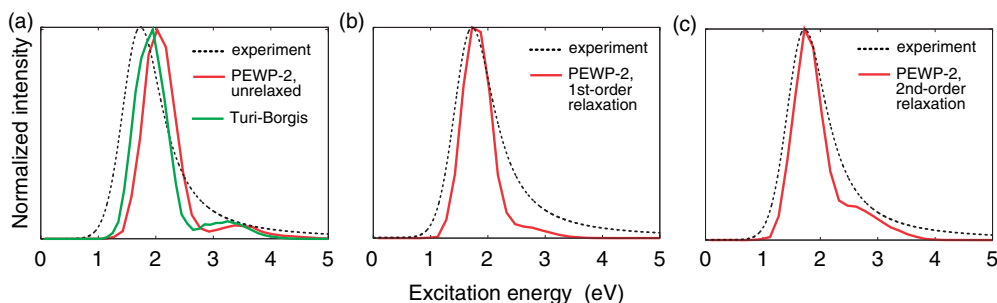


Figure 14 (colour online). Comparisons of the experimental electronic absorption spectrum of $e^-(aq)$, obtained using line-shape parameters from Ref. [93], to spectra simulated using the Turi-Borgis one-electron model [49], as well as our own PEWP-2 model. In the latter case, we show results from three different treatments of electronic relaxation: (a) complete neglect of relaxation, *i.e.*, only ground-state dipoles are used; (b) a first-order treatment of the relaxation, using the state-specific perturbation \hat{W}_n introduced in Equation (22); and (c) a second-order treatment of \hat{W}_n . The PEWP-2 simulations were carried out using a periodic simulation cell containing 600 water molecules; spectra are computed using the first 29 excited states.

invariant to translation of the coordinate origin, although the sum rule may still be violated. In practice, we find that $\langle \psi_m | \psi_n \rangle \lesssim 0.1$ for $m \neq n$.

Figure 14 compares the experimental absorption spectrum for $e^-(aq)$ to spectra computed using various corrections for the perturbation \hat{W}_n . The “unrelaxed” spectrum corresponds to a complete neglect of \hat{W}_n , so that only ground-state dipoles are used in the calculation, whereas “relaxed” spectra include either a first- or second-order correction for \hat{W}_n .

The unrelaxed PEWP-2 spectrum, Figure 14(a), is quite similar to the spectrum obtained using the Turi-Borgis (TB) hydrated-electron model [49,79]. Among the non-polarizable one-electron models that have been introduced over the years, the TB model affords the closest agreement with the experimentally-observed absorption maximum, although even this model predicts a peak that is blue-shifted (relative to experiment) by about 0.3 eV. Turi and co-workers [49,216] have claimed that a proper treatment of excited-state polarization would red-shift the spectrum by 0.2–0.3 eV, and this hypothesis is confirmed by the spectrum shown in Figure 14(b). First-order relaxation shifts the absorption maximum of the PEWP-2 model into nearly perfect agreement with experiment.

The line shape of the experimental absorption spectrum for $e^-(aq)$ is fit very well by a function that is a Gaussian on the red side of the spectrum (below 1.72 eV) and a Lorentzian on the blue side [93]. The first-order relaxed spectrum affords a reasonable description of the low-energy Gaussian feature, as does the TB model (albeit slightly blue-shifted). The consensus view, based upon simulations using various one-electron models [34,35,49,79] as well as all-electron *ab initio* calculations [128,149,192] is that this Gaussian feature arises from three $s \rightarrow p$ excitations of a particle in an asymmetrical solvent cavity. On the other hand, none of these models recovers anything resembling the “blue tail” seen in the experimental spectrum. Within the PEWP-2 model, a first-order treatment of electronic relaxation dramatically red-shifts the spectrum, and also smoothes out the line shape. However the blue tail is absent at first order.

A second-order treatment of the dipole relaxation is required in order to obtain a blue tail. To understand why, consider that we calculate spectra as histograms of excitation energies, binned over ~ 1000 snapshots extracted from a bulk simulation and weighted by oscillator strengths, $f_{0 \rightarrow n}$ [146]:

$$f_{0 \rightarrow n} = \frac{2m_e}{3\hbar^2} (E_n - E_0) \left(|\langle \psi_n | \hat{x} | \psi_0 \rangle|^2 + |\langle \psi_n | \hat{y} | \psi_0 \rangle|^2 + |\langle \psi_n | \hat{z} | \psi_0 \rangle|^2 \right). \quad (23)$$

Owing to the factor of $E_n - E_0$ in this expression, first-order relaxation actually *diminishes* the oscillator strength in the blue tail, since the excited-state energies are stabilized by electronic relaxation of the solvent. At second order, one also obtains a correction to the transition dipoles. As seen in Figure 14(c), the second-order treatment of relaxation significantly enhances the oscillator strength on the blue edge of spectrum, providing a substantial “blue tail”, without the gap in intensity around 2.5–3.0 eV that is seen in the absence of excited-state dipole relaxation.

To understand this in more detail, Figure 15 decomposes the absorption spectrum, computed in various ways, into contributions from different categories of excited states. Consistent with the results of many previous simulations [34,35,49,79,128,149] nearly all of the oscillator strength is carried by the three $1p$ states, which can be understood in terms of a simple particle-in-a-cavity model. A potential energy function of the form

$$V(r) = \begin{cases} 0, & r \leq 3.7 \text{ \AA} \\ 5.25 \text{ eV}, & r > 3.7 \text{ \AA} \end{cases} \quad (24)$$

affords a VEBE of 3.5 eV, a radius of gyration $r_g = 2.5 \text{ \AA}$, and a $1s \rightarrow 1p$ excitation energy of 1.7 eV, each of which is in good agreement with experimental data. In such a model, only the $1s$ and $1p$ states are bound, and the three $1s \rightarrow 1p$ excitations carry 98.7% of the oscillator strength. In the atomistic simulations, each of these three excitations gives rise to a broad Gaussian profile, and together these states provide a reasonable description of the Gaussian part of the experimental spectrum. At slightly higher excitation energies, however, both the unrelaxed PEWP-2 model and the non-polarizable TB model predict an intensity gap, just below 3 eV on the blue edge of the $1s \rightarrow 1p$ band. Above this gap is a weak tail comprised of excitations to unbound states,¹² *i.e.*, a photo-electron spectrum.

First-order relaxation [Figure 15(c)] not only shifts the absorption maximum into agreement with experiment, it also red-shifts the higher-lying states to a greater extent than the $1p$ states, resulting in a smoother decay of the spectrum at high energy, without so much of the aforementioned gap in intensity. However, the blue tail remains largely absent because the zeroth-order $1p$ states, which carry most of the oscillator strength, do not mix with the higher-energy states. Such mixing *can* occur at second order, and second-order relaxation thereby facilitates intensity borrowing by the higher-lying states. The result [Figure 15(d)] is a significant intensity enhancement in the blue tail. This is consistent with the TD-DFT calculations discussed in Section 2.1.2, where we found that a sizable QM region was necessary in order to recover a blue tail [128]. This observation supports the idea that solvent polarization upon electronic excitation facilitates intensity borrowing by the higher-energy states.

At the same time, the $1p$ states are still readily identifiable as such, even following second-order relaxation, and these states are still clearly responsible for the Gaussian feature in the absorption spectrum. Second-order relaxation does have a qualitative effect

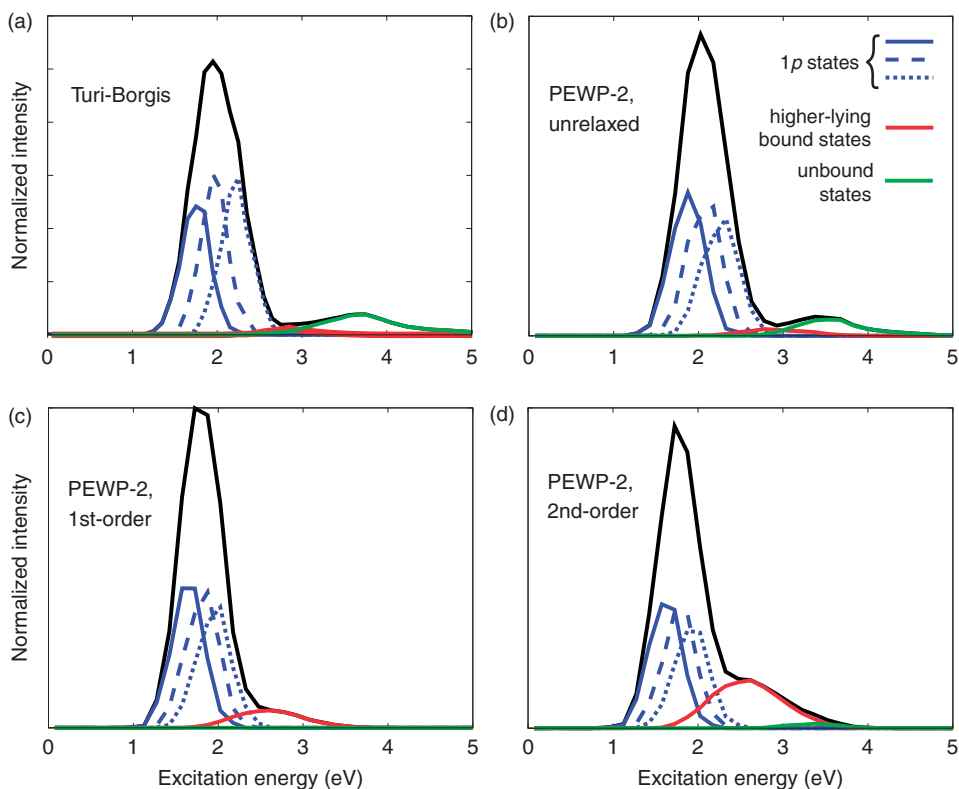


Figure 15 (colour online). Simulated absorption spectra for $e^-(aq)$, decomposed into contributions from various types of excited states: (a) the Turi-Borgis spectrum, (b) the unrelaxed PEWP-2 spectrum, (c) the first-order relaxed PEWP-2 spectrum, and (d) the second-order relaxed PEWP-2 spectrum. A total of 29 excited states are used to construct each spectrum, and we categorize these states as bound or unbound based upon whether the excitation energy is less than or greater than the VEBE. The Gaussian ($1p$) portion of the spectrum is converged even in modest simulation cells containing 100 water molecules, whereas the PEWP-2 spectra shown here were obtained using a 600-molecule simulation cell, which is necessary in order to converge the blue edge of the spectrum [116]. (Adapted from Ref. [116], incorporating some additional data here; copyright 2010 American Institute of Physics.)

on the orientation of the $1s \rightarrow 1p$ transition dipoles, however. At zeroth order, these transition dipoles are mutually perpendicular (as they are in the particle-in-a-cavity model), but at second order they exhibit angles as large as 60° between one another [116]. In our view, this helps to explain why the aqueous electron fails to exhibit any polarization-dependent bleaching dynamics in polarized transient hole-burning experiments [217–219]. The absence of such dynamics has long been an open question in $e^-(aq)$ spectroscopy, since non-polarizable one-electron models predict that such dynamics should be observable [59,61] but if the transition dipoles start out far from perpendicular then they may depolarize too rapidly for anisotropic bleaching dynamics to be observed [116].

Another consequence of second-order relaxation is that it leads to a significant increase in the number of (vertically) bound states, from 6.9 bound states (on average) when relaxation is neglected, to 25.6 at second order.¹³ This is why the feature labeled “unbound

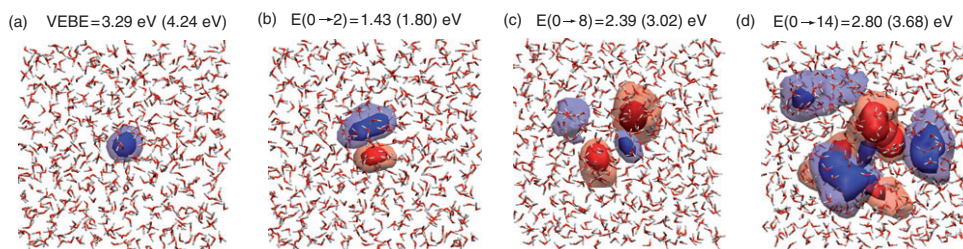


Figure 16 (colour online). Typical examples of (a) the ground-state and (b)–(d) excited-state e^- wavefunctions, calculated in bulk water using the PEWP-2 model. Relaxed values of the VEBE and excitation energies for this particular snapshot are also shown, with unrelaxed values given in parentheses. The translucent isosurfaces encompass 60% of the total probability density, $|\psi|^2$, whereas the opaque isosurfaces encapsulate 90%.

states” is almost completely absent in the second-order spectrum; there are so many *bound* states in this case that we simply have not calculated enough states to describe this feature properly. (The states that we do calculate account for about 90% of the total oscillator strength.)

Historically, the blue tail in the absorption spectrum has been discussed exclusively in terms of bound \rightarrow continuum transitions [35,79,220], but our results suggest that there may exist (vertically) bound states beyond the $1p$ manifold that possess some particle-in-a-cavity character. One such example is shown in Figure 16(c). In contrast, the state shown in Figure 16(d) is much more delocalized, to the point that it is difficult to assign particle-in-a-cavity quantum numbers, although this state remains bound in the vertical sense. The delocalization evident in Figure 16(d) is what one would expect for states that lie just below the finite binding energy of the cavity, and which therefore inherit some continuum-like character. We note that in our simulations, the manifold of $1p$ states extends no higher than about 2.5 eV, whereas unbound excitations appear at 3.0–3.5 eV. In the narrow window in between, the excited states must evolve from compact, particle-in-a-cavity wavefunctions [as in Figure 16(b)] into completely delocalized plane waves. It is the states in this intermediate region that comprise the blue tail. We call these “polarization-bound, quasi-continuum states” [128], because they are bound only by electronic re-organization following excitation of the electron. Such states, an example of which is depicted in Figure 16(d), are conspicuously absent in non-polarizable simulations, as is the blue tail.

The extent to which these quasi-continuum states are delocalized can be quantified by calculating their radii of gyration, which are plotted in Figure 17(a) as a function of the size of the periodic simulation cell. It is worth noticing that the wavefunctions for the $1p$ states are considerably more compact ($r_g = 4.0\text{--}4.5 \text{ \AA}$) than are the higher-energy states ($r_g > 6.5 \text{ \AA}$). As such, there exists a notable gap in r_g above the $1p$ -manifold, even though there is not much of a gap in the average excitation energies [Figure 17(b)]. In fact, the band labeled “higher-lying bound states” in Figure 15(d) reaches all the way down to the absorption maximum at 1.7 eV. It is interesting to speculate whether the disjoint lobes seen in some of these higher-lying states [*e.g.*, the ones shown in Figure 16(c) and (d)] could facilitate excited-state electron “hopping” and thereby explain excited-state $e^-(aq)$ migration. (Such migration is usually explained in terms of conduction-band states [220].) Such a hopping process might play a role in biological radiation damage by

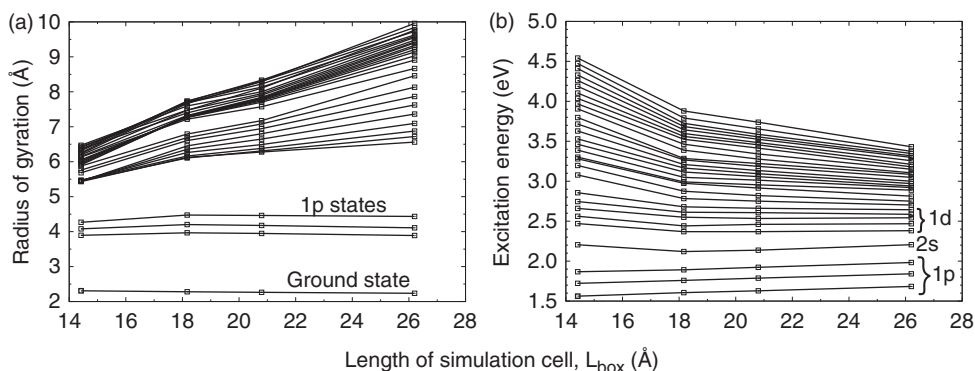


Figure 17. (a) Ground- and excited-state radii of gyration, and (b) vertical excitation energies for $e^-(aq)$, as a function of the size of the periodic simulation cell. The data points represent averages over a molecular dynamics simulation. (Reprinted from Ref. [116]; copyright 2010 American Institute of Physics.)

low-energy electrons [17–20,221–223], via dissociative electron attachment [223], and thus warrants further investigation.

Although the high-energy edge of our computed spectrum is not in quantitative agreement with experiment, it is vastly improved relative to what is predicted using non-polarizable models. We note that our calculations do not include any sort of lifetime broadening, which could be important given the high spectral density beyond the $1p$ manifold [see Figure 17(b)]. Dynamics among these excited states might be the origin of the Lorentzian line shape that is observed experimentally. This hypothesis is supported by the fact that the Lorentzian line shape parameters (which describe the blue side of the spectrum) are slightly different in D_2O than in H_2O , whereas the Gaussian line shape parameters (which describe the red side) are the same [93].

Another source of error in the PEWP-2 line shape on the blue edge of the spectrum is that our model includes the solvent’s contribution to the oscillator strengths only indirectly, via the response of the electron’s wavefunction to changes in the MM dipole parameters. In a fully-QM treatment, the H_2O dipole moments would contribute to the dipole moment operator in Equation (23). Shkrob *et al.* [149] have reported QM/MM calculations of the $e^-(aq)$ absorption spectrum, at the level of singles configuration interaction (CIS), but these calculations did not result in a blue tail. These authors acknowledge that the higher-lying states are quite diffuse, and it is unclear whether the QM region in these calculations is sufficient to describe these states. The blue tail is also absent in the Kohn-Sham density of states obtained from a Car-Parrinello simulation of $e^-(aq)$ [192]. We find that a sizable QM region (somewhat larger than that used by Shkrob *et al.* [149]) is required in order to obtain this tail, which we interpret as evidence that solvent polarization does indeed facilitate intensity borrowing by higher-lying excited states.

5. Summary

The success of our PEWP-2 hydrated-electron model [116], for both cluster and bulk benchmarks, suggests that we have successfully found a “middle way” that is more accurate than non-polarizable one-electron models, yet is affordable enough to be applied

to very large $(\text{H}_2\text{O})_n^-$ clusters and to $e^-(aq)$ in bulk solution using large, periodic simulation cells. It is certainly true that some aspects of electron solvation cannot be understood within a strictly one-electron model [145,148,152], and *ab initio* calculations suggest that 10–20% of the spin density in these systems is carried by frontier MOs on the water molecules [148,152]. Nevertheless, the PEWP-2 model does afford VEBEs that are in far better agreement (~ 0.1 eV) with *ab initio* benchmarks than previous models, across a wide range of binding energies (0–2.5 eV). Relative conformational energies are also reproduced within ~ 1 kcal/mol, for both neutral and anionic water clusters, and in regions of the potential surface where the neutral isomers are highly unstable. These observations suggest that the PEWP-2 model can provide a *quantitative* account of cluster photoelectron experiments. Efforts to simulate such experiments are currently underway in our group.

For the aqueous electron in bulk water, we find that solvent polarization plays a qualitatively important role in the spectroscopy. Relaxation of the solvent's electrostatic degrees of freedom, upon detachment of the electron, reduces the bulk value of the *vertical* electron binding energy (prior to any nuclear dynamics) by about 1.4 eV. In a sense, this is a many-electron effect, insofar as the H_2O polarization degrees of freedom are electronic in nature, and it is an effect that is absent in non-polarizable one-electron models. While a non-polarizable model could conceivably be parameterized to reproduce an experimental value for the bulk VEBE, it is difficult to imagine that such a model could afford accurate VEBEs in both $(\text{H}_2\text{O})_n^-$ clusters and bulk solution. Indeed, we find that the TB non-polarizable model [49] is underbinding by an average of 0.25 eV in $(\text{H}_2\text{O})_n^-$ clusters ($n \leq 33$), yet overbinding by at least 1.2 eV in bulk solution [116].

A second key effect of the solvent polarization response is that it leads to many additional bound states in the excitation spectrum, and furthermore facilitates intensity borrowing from the $1p$ states that carry essentially all of the oscillator strength, in the absence of the solvent's polarization response. This leads to a "blue tail" in the electronic absorption spectrum of $e^-(aq)$, which is seen experimentally but is absent in all previous calculations based upon one-electron models [128]. The higher-lying bound states that comprise this tail are significantly more diffuse than the $1p$ states, which may have interesting consequences for the photophysics of $e^-(aq)$. Along the same lines, $e^-(aq)$ can be formed via charge-transfer-to-solvent excitation of aqueous halide ions [224], and the role of solvent polarization in this process has yet to be explored. These aspects of electron solvation warrant further consideration in the future.

Acknowledgments

We thank J.V. Coe, S.E. Bradforth, and M.A. Johnson for many insightful discussions. We also thank A.E. Bragg for providing an electronic copy of the data in Figure 2(a) and B.J. Schwartz for providing a preprint of Ref. [56]. Some of the early results discussed herein were obtained in collaboration with M. Head-Gordon and C.F. Williams. This work has been supported financially by the National Science Foundation, the American Chemical Society's Petroleum Research Fund, the Alfred P. Sloan Foundation, and The Ohio State University, and by allocations of computer time at the Ohio Supercomputer Center. Isoprobability contour values were calculated using the OpenCubMan program [225] and rendered with the Visual Molecular Dynamics program [226]. All-electron calculations were performed using a locally-modified version of Q-Chem [174]. Version 4.2 of the TINKER program, as distributed by J.W. Ponder (<http://dasher.wustl.edu/tinker>) was used to interface the AMOEBA water model with our own simulation codes.

Notes

1. Histories of the early developments in this field can be found in Refs. [11] and [12]. A recent overview of the chemical and physical properties of $e^-(aq)$ can be found in Ref. [13].
2. Robinson *et al.* [121,122] long ago suggested that H_3O might actually be part of the molecular-level structure of $e^-(aq)$, although in their picture, the so-called aqueous electron was really a $OH^- \cdots H_3O$ complex.
3. Most DFT methods severely overbind the excess electron, owing to spurious self-interaction error [44].
4. The TD-DFT calculations of the $e^-(aq)$ absorption spectrum were actually run with $\mu = 0.37 a_0^{-1}$, whereas the VEBE benchmarks with this functional employ $\mu = 0.33 a_0^{-1}$. However, the slightly altered value of μ makes little difference in the computed excitation energies [128].
5. A quantitative reproduction of the high-energy tail is probably impossible using all-electron quantum mechanics, due to the large extent of these excited states. In the one-electron calculations discussed in Section 4.2, we use dense, real-space grids in a periodic simulation cell containing 600 water molecules, yet the radii of gyration for the highest-energy states are still not completely converged with respect to the size of the box [116].
6. For gas-phase cluster calculations, we prefer the 6-31(1+,3+)G* basis set, which includes one set of diffuse *s* and *p* functions on the oxygen atoms and three sets of diffuse *s* functions on the hydrogen atoms, with exponents as defined in Refs. [44] and [139]. We have found that VEBEs computed with this basis set lie within 0.02–0.03 eV of those obtained using larger, more diffuse basis sets, even for the weakest-binding cluster isomers [44]. It is worth noting, however, that even the first set of diffuse basis functions on hydrogen have a full width at half maximum of 2.3 Å, which is larger than the distance between water molecules.
7. Although the “particle in a spherical box” wavefunctions qualitatively resemble hydrogen-atom wavefunctions, the angular momentum quantum number in the spherical-box problem is not bounded by the principal quantum number. The energy levels increase in the order $E(1s) < E(1p) < E(1d) < E(2s) < \cdots$, although the 1*d* and 2*s* levels are relatively close in energy, within the spherical cavity model [180], and the order of these states is reversed in the particular TD-DFT snapshot shown in Figure 6(b).
8. The lowest-energy $(H_2O)_{20}$ structure that we obtain using the SPC model is essentially the same as that obtained using the TIP3P water model [191].
9. One must always bear in mind that the wavefunction has a significant tail that, according to our calculations, penetrates into at least the second solvation shell. Nevertheless, the wavefunction in Figure 1(c) is clearly cavity-centered.
10. A small number of hydrated-electron models that include many-body polarization have been reported previously [30,53,132]. However, none of these models has been thoroughly benchmarked, nor has any been used to examine the solvent polarization response following electron detachment or electronic excitation.
11. If the HOMO/LUMO gap is large compared to the relaxation energy, which is likely to be the case in uncharged molecular systems, we anticipate that serious convergence problems can be avoided.
12. We categorize the excited states as bound or unbound in the vertical sense, based upon whether the excitation energy exceeds the energy required to remove the electron *when the positions of the water molecules are fixed*. We make no claims as to whether these states are adiabatically bound or not.
13. The number of bound states is quite sensitive to the size of the simulation cell. For a simulation cell containing 100 water molecules, only 9.3 excited states are bound, on average, using second-order relaxation.

References

- [1] C. A. Kraus, J. Am. Chem. Soc. **29**, 1557 (1907).
- [2] C. A. Kraus, J. Am. Chem. Soc. **30**, 1323 (1908).

- [3] C. A. Kraus, *J. Am. Chem. Soc.* **36**, 864 (1914).
- [4] C. A. Kraus, *J. Am. Chem. Soc.* **43**, 749 (1921).
- [5] G. E. Gibson and W. L. Argo, *J. Am. Chem. Soc.* **40**, 1327 (1918).
- [6] G. Stein, *Discuss. Faraday Soc.* 227 (1952).
- [7] R. L. Platzman, *Physical and Chemical Aspects of Basic Mechanisms in Radiobiology* (Technical Report 305, US National Research Council, Washington, DC, 1953).
- [8] F. P. Sargent and E. M. Gardy, *Chem. Phys. Lett.* **39**, 188 (1976).
- [9] E. J. Hart and J. W. Boag, *J. Am. Chem. Soc.* **84**, 4090 (1962).
- [10] J. W. Boag and E. J. Hart, *Nature* **197**, 45 (1963).
- [11] E. J. Hart and M. Anbar, *The Hydrated Electron* (John Wiley, New York, 1970).
- [12] J. W. Boag, in *Early Developments in Radiation Chemistry*, edited by J. Kroh (Royal Society of Chemistry, Cambridge, 1989), pp. 7–20.
- [13] M. Mostafavi and I. Lampre, in *Radiation Chemistry*, edited by M. Spothem-Maurizot, M. Mostafavi, J. Belloni, and T. Douki (EDP Sciences, 2008), chapter 3, pp. 33–52.
- [14] E. J. Hart (ed.), *Solvated Electron, Volume 50 of Advances in Chemistry* (American Chemical Society, Washington, DC, 1965).
- [15] G. V. Buxton, C. L. Greenstock, W. P. Helman, and A. B. Ross, *J. Phys. Chem. Ref. Data* **17**, 513 (1988).
- [16] B. C. Garrett, D. A. Dixon, D. M. Camaioni, D. M. Chipman, M. A. Johnson, C. D. Jonah, G. A. Kimmel, J. H. Miller, T. N. Rescigno, P. J. Rossky, S. S. Xantheas, S. D. Colson, A. H. Laufer, D. Ray, P. F. Barbara, D. M. Bartels, K. H. Becker, K. H. Bowen Jr, S. E. Bradforth, I. Carmichael, J. V. Coe, L. R. Corrales, J. P. Cowin, M. Dupuis, K. B. Eisenthal, J. A. Franz, M. S. Gutowski, K. D. Jordan, B. D. Kay, J. A. LaVerne, S. V. Lymar, T. E. Madey, C. W. McCurdy, D. Meisel, S. Mukamel, A. R. Nilsson, T. M. Orlando, N. G. Petrik, S. M. Pimblott, J. R. Rustad, G. K. Schenter, S. J. Singer, A. Tokmakoff, L.-S. Wang, C. Wittig, and T. S. Zwier, *Chem. Rev.* **105**, 355 (2005).
- [17] C.-R. Wang and Q.-B. Lu, *Angew. Chem. Int. Ed. Engl.* **46**, 6316 (2007).
- [18] Y. Gauduel, Y. Glinec, and V. Malka, *J. Phys. Conf. Ser.* **101**, 012004 (2008).
- [19] C.-R. Wang, J. Nguyen, and Q.-B. Lu, *J. Am. Chem. Soc.* **131**, 11320 (2009).
- [20] Q.-B. Lu, *Mutat. Res.* **704**, 190 (2010).
- [21] K. D. Jordan and F. Wang, *Annu. Rev. Phys. Chem.* **54**, 367 (2003).
- [22] B. J. Berne and D. Thirumalai, *Annu. Rev. Phys. Chem.* **37**, 401 (1986).
- [23] M. Parrinello and A. Rahman, *J. Chem. Phys.* **80**, 860 (1984).
- [24] M. Sprik, R. W. Impey, and M. L. Klein, *J. Chem. Phys.* **83**, 5802 (1985).
- [25] M. Sprik, R. W. Impey, and M. L. Klein, *J. Stat. Phys.* **43**, 967 (1986).
- [26] M. Sprik and M. L. Klein, *Comput. Phys. Rep.* **7**, 147 (1988).
- [27] C. D. Jonah, C. Romero, and A. Rahman, *Chem. Phys. Lett.* **123**, 209 (1986).
- [28] D. Thirumalai, A. Wallqvist, and B. J. Berne, *J. Stat. Phys.* **43**, 973 (1986).
- [29] A. Wallqvist, D. Thirumalai, and B. J. Berne, *J. Chem. Phys.* **85**, 1583 (1986).
- [30] A. Wallqvist, D. Thirumalai, and B. J. Berne, *J. Chem. Phys.* **86**, 6404 (1987).
- [31] A. Wallqvist, G. Martyna, and B. J. Berne, *J. Phys. Chem.* **92**, 1721 (1988).
- [32] P. J. Rossky, J. Schnitker, and R. A. Kuharski, *J. Stat. Phys.* **43**, 949 (1986).
- [33] J. Schnitker and P. J. Rossky, *J. Chem. Phys.* **86**, 3471 (1987).
- [34] J. Schnitker, K. Motakabbir, P. J. Rossky, and R. A. Friesner, *Phys. Rev. Lett.* **60**, 456 (1988).
- [35] P. J. Rossky and J. Schnitker, *J. Phys. Chem.* **92**, 4277 (1988).
- [36] J. Schnitker and P. J. Rossky, *J. Phys. Chem.* **93**, 6965 (1989).
- [37] U. Landman, R. N. Barnett, C. L. Cleveland, D. Scharf, and J. Jortner, *J. Phys. Chem.* **91**, 4890 (1987).
- [38] R. N. Barnett, U. Landman, and C. L. Cleveland, *Phys. Rev. Lett.* **59**, 811 (1987).
- [39] R. N. Barnett, U. Landman, C. L. Cleveland, and J. Jortner, *J. Chem. Phys.* **88**, 4429 (1988).
- [40] R. N. Barnett, U. Landman, and C. L. Cleveland, *Chem. Phys. Lett.* **145**, 382 (1988).

- [41] R. N. Barnett, U. Landman, D. Scharf, and J. Jortner, *Acc. Chem. Res.* **22**, 350 (1989).
- [42] R. N. Barnett, U. Landman, and A. Nitzan, *J. Chem. Phys.* **89**, 2242 (1988).
- [43] H. Haberland, H. Langosch, H. G. Schindler, and D. R. Worsnop, *J. Phys. Chem.* **88**, 3903 (1984).
- [44] J. M. Herbert and M. Head-Gordon, *J. Phys. Chem. A* **109**, 5217 (2005).
- [45] J. Schnitker and P. J. Rossky, *J. Chem. Phys.* **86**, 3462 (1987).
- [46] C. J. Smallwood, R. E. Larsen, W. J. Glover, and B. J. Schwartz, *J. Chem. Phys.* **125**, 074102 (2006).
- [47] I. Park, K. Cho, S. Lee, K. S. Kim, and J. D. Joannopoulos, *Comp. Mat. Sci.* **21**, 291 (2001).
- [48] L. Turi, M.-P. Gaigeot, N. Levy, and D. Borgis, *J. Chem. Phys.* **114**, 7805 (2001).
- [49] L. Turi and D. Borgis, *J. Chem. Phys.* **117**, 6186 (2002).
- [50] F. Wang and K. D. Jordan, *J. Chem. Phys.* **116**, 6973 (2002).
- [51] T. Sommerfeld and K. D. Jordan, *J. Phys. Chem. A* **109**, 11531 (2005).
- [52] T. Sommerfeld, A. DeFusco, and K. D. Jordan, *J. Phys. Chem. A* **112**, 11021 (2008).
- [53] J. E. Aremu-Cole, *Mixed Quantum-Classical Study of a Hydrated Electron and Investigation of Temperature-Control Algorithms*, PhD thesis, Clemson University, 2007.
- [54] L. D. Jacobson, C. F. Williams, and J. M. Herbert, *J. Chem. Phys.* **130**, 124115 (2009).
- [55] R. E. Larsen, W. J. Glover, and B. J. Schwartz, *J. Chem. Phys.* **131**, 037101 (2009).
- [56] R. E. Larsen, W. J. Glover, and B. J. Schwartz, *Science* **329**, 65 (2010).
- [57] M. Sprik, *J. Phys.-Condens. Mat.* **2**, SA161 (1990).
- [58] B. J. Schwartz and P. J. Rossky, *J. Chem. Phys.* **101**, 6902 (1994).
- [59] B. J. Schwartz and P. J. Rossky, *J. Chem. Phys.* **101**, 6917 (1994).
- [60] B. J. Schwartz and P. J. Rossky, *J. Phys. Chem.* **98**, 4439 (1994).
- [61] B. J. Schwartz and P. J. Rossky, *Phys. Rev. Lett.* **72**, 3282 (1994).
- [62] J. Jortner, U. Landman, and R. N. Barnett, *Chem. Phys. Lett.* **152**, 353 (1988).
- [63] C. Romero and C. D. Jonah, *J. Chem. Phys.* **90**, 1877 (1989).
- [64] C.-Y. Yang, F. Kim, M. S. Skaf, and P. J. Rossky, *J. Chem. Phys.* **114**, 3598 (2001).
- [65] M. Skorobogatiy, I. J. Park, and J. D. Joannopoulos, *Comp. Mat. Sci.* **32**, 96 (2005).
- [66] C. Nicolas, A. Boutin, B. Levy, and D. Borgis, *J. Chem. Phys.* **118**, 9689 (2003).
- [67] K. A. Tay and A. Boutin, *J. Phys. Chem. B* **113**, 11943 (2009).
- [68] F. Wang and K. D. Jordan, *J. Chem. Phys.* **119**, 6973 (2003).
- [69] T. Sommerfeld and K. D. Jordan, *J. Am. Chem. Soc.* **128**, 5828 (2006).
- [70] T. Sommerfeld, S. D. Gardner, A. DeFusco, and K. D. Jordan, *J. Chem. Phys.* **125**, 174301 (2006).
- [71] A. DeFusco, T. Sommerfeld, and K. D. Jordan, *Chem. Phys. Lett.* **455**, 135 (2008).
- [72] T. H. Choi and K. D. Jordan, *Chem. Phys. Lett.* **475**, 293 (2009).
- [73] L. Turi, W.-S. Sheu, and P. J. Rossky, *Science* **309**, 914 (2005).
- [74] L. Turi, Á. Madarász, and P. J. Rossky, *J. Chem. Phys.* **125**, 014308 (2006).
- [75] D. Borgis, P. J. Rossky, and L. Turi, *J. Chem. Phys.* **125**, 064501 (2006).
- [76] D. Borgis, P. J. Rossky, and L. Turi, *J. Chem. Phys.* **127**, 174508 (2007).
- [77] Á. Madarász, P. J. Rossky, and L. Turi, *J. Chem. Phys.* **126**, 234707 (2007).
- [78] A. Madarasz, P. J. Rossky, and L. Turi, *J. Chem. Phys.* **130**, 124319 (2009).
- [79] L. Turi, G. Hantal, P. J. Rossky, and D. Borgis, *J. Chem. Phys.* **131**, 024119 (2009).
- [80] A. Madarasz, P. J. Rossky, and L. Turi, *J. Phys. Chem. A* **114**, 2331 (2010).
- [81] D. M. Neumark, *Mol. Phys.* **106**, 2183 (2008).
- [82] J. V. Coe, G. H. Lee, J. G. Eaton, S. T. Arnold, H. W. Sarkas, K. H. Bowen, C. Ludewigt, H. Haberland, and D. R. Worsnop, *J. Chem. Phys.* **92**, 3960 (1990).
- [83] G. H. Lee, S. T. Arnold, H. W. Sarkas, K. H. Bowen, C. Ludewigt, and H. Haberland, *Z. Phys. D Atom. Mol. Cl.* **20**, 9 (1991).
- [84] J. R. R. Verlet, A. E. Bragg, A. Kamrath, O. Cheshnovsky, and D. M. Neumark, *Science* **307**, 93 (2005).

- [85] J. Kim, I. Becker, O. Cheshnovsky, and M. A. Johnson, *Chem. Phys. Lett.* **297**, 90 (1998).
- [86] J.-W. Shin, N. I. Hammer, J. M. Headrick, and M. A. Johnson, *Chem. Phys. Lett.* **399**, 349 (2004).
- [87] N. I. Hammer, J. R. Roscioli, and M. A. Johnson, *J. Phys. Chem. A* **109**, 7896 (2005).
- [88] R. N. Barnett, U. Landman, C. L. Cleveland, and J. Jortner, *J. Chem. Phys.* **88**, 4421 (1988).
- [89] A. Kammrath, J. R. R. Verlet, G. B. Griffin, and D. M. Neumark, *J. Chem. Phys.* **125**, 076101 (2006).
- [90] J. V. Coe, S. T. Arnold, J. G. Eaton, G. H. Lee, and K. H. Bowen, *J. Chem. Phys.* **125**, 014315 (2006).
- [91] A. A. Rashin and B. Honig, *J. Phys. Chem.* **89**, 5588 (1985).
- [92] X.-J. Wang, Q. Zhu, Y.-K. Li, X.-M. Cheng, X.-Y. Li, K.-X. Fu, and F.-C. He, *J. Phys. Chem. B* **114**, 2189 (2010).
- [93] J. V. Coe, S. M. Williams, and K. H. Bowen, *Int. Rev. Phys. Chem.* **27**, 27 (2008).
- [94] A. E. Bragg, J. R. R. Verlet, A. Kammrath, O. Cheshnovsky, and D. M. Neumark, *Science* **306**, 669 (2004).
- [95] A. E. Bragg, J. R. R. Verlet, A. Kammrath, O. Cheshnovsky, and D. M. Neumark, *J. Am. Chem. Soc.* **127**, 15283 (2005).
- [96] Y. Tang, H. Shen, K. Sekiguchi, N. Kurahashi, T. Mizuno, Y. I. Suzuki, and T. Suzuki, *Phys. Chem. Chem. Phys.* **12**, 3653 (2010).
- [97] K. R. Siefertmann, Y. Liu, E. Lugovoy, O. Link, M. Faubel, U. Buck, B. Winter, and B. Abel, *Nat. Chem.* **2**, 274 (2010).
- [98] A. T. Shreve, T. A. Yen, and D. M. Neumark, *Chem. Phys. Lett.* **493**, 216 (2010).
- [99] L. Ma, K. Majer, F. Chiro, and B. von Issendorff, *J. Chem. Phys.* **131**, 144303 (2009).
- [100] R. N. Barnett, U. Landman, G. Makov, and A. Nitzan, *J. Chem. Phys.* **93**, 6226 (1990).
- [101] D. M. Bartels, *J. Chem. Phys.* **115**, 4404 (2001).
- [102] A. Kammrath, J. R. R. Verlet, A. E. Bragg, G. B. Griffin, and D. M. Neumark, *J. Phys. Chem. A* **109**, 11475 (2005).
- [103] J. R. R. Verlet, A. Kammrath, G. B. Griffin, and D. M. Neumark, *J. Chem. Phys.* **123**, 231102 (2005).
- [104] O. Marsalek, F. Uhlig, T. Frigato, B. Schmidt, and P. Jungwirth, *Phys. Rev. Lett.* **105**, 043002 (2010).
- [105] P. Ayotte, C. G. Bailey, J. Kim, and M. A. Johnson, *J. Chem. Phys.* **108**, 444 (1998).
- [106] N. I. Hammer, J. W. Shin, J. M. Headrick, E. G. Diken, J. R. Roscioli, G. H. Weddle, and M. A. Johnson, *Science* **306**, 675 (2004).
- [107] N. I. Hammer, J. R. Roscioli, M. A. Johnson, E. M. Myshakin, and K. D. Jordan, *J. Phys. Chem. A* **109**, 11526 (2005).
- [108] J. R. Roscioli, N. I. Hammer, and M. A. Johnson, *J. Phys. Chem. A* **110**, 7517 (2006).
- [109] H. M. Lee, S. Lee, and K. S. Kim, *J. Chem. Phys.* **119**, 187 (2003).
- [110] J. M. Herbert and M. Head-Gordon, *Proc. Natl. Acad. Sci. USA* **103**, 14282 (2006).
- [111] N. I. Hammer, J. R. Roscioli, J. C. Bopp, J. M. Headrick, and M. A. Johnson, *J. Chem. Phys.* **123**, 244311 (2005).
- [112] K. R. Asmis, G. Santabrogio, J. Zhou, E. Garand, J. Headrick, D. Goebbert, M. A. Johnson, and D. M. Neumark, *J. Chem. Phys.* **126**, 191105 (2007).
- [113] M. J. Tauber and R. A. Mathies, *J. Am. Chem. Soc.* **125**, 1394 (2003).
- [114] J. M. Herbert, L. D. Jacobson, and C. F. Williams, in *Molecular Potential Energy Surfaces in Many Dimensions*, edited by M. M. Law and A. Ernesti (Daresbury, United Kingdom, 2009), pp. 28–38.
- [115] J. Jortner and S. A. Rice, in *Solvated Electron*, edited by R. F. Gould, *Volume 50 of Advances in Chemistry* (American Chemical Society Publications, Washington, DC, 1965), chapter 2, pp. 7–26.
- [116] L. D. Jacobson and J. M. Herbert, *J. Chem. Phys.* **133**, 154506 (2010).

- [117] A. L. Sobolewski and W. Domcke, *Phys. Chem. Chem. Phys.* **4**, 4 (2002).
- [118] A. L. Sobolewski and W. Domcke, *J. Phys. Chem. A* **106**, 4158 (2002).
- [119] S. Neumann, W. Eisfeld, A. Sobolewski, and W. Domcke, *Phys. Chem. Chem. Phys.* **6**, 5297 (2004).
- [120] A. L. Sobolewski and W. Domcke, *Phys. Chem. Chem. Phys.* **9**, 3818 (2007).
- [121] G. W. Robinson, P. J. Thistlewaite, and J. Lee, *J. Phys. Chem.* **90**, 4224 (1986).
- [122] H. F. Hameka, G. W. Robinson, and C. J. Marsden, *J. Phys. Chem.* **91**, 3150 (1987).
- [123] L. Kevan, *J. Phys. Chem.* **85**, 1628 (1981).
- [124] L. Kevan, *Acc. Chem. Res.* **14**, 138 (1981).
- [125] P. Han and D. M. Bartels, *J. Phys. Chem.* **95**, 5367 (1991).
- [126] P. Han and D. M. Bartels, *J. Phys. Chem.* **94**, 7294 (1990).
- [127] Y. Zhang and P. S. Cremer, *Curr. Opin. Chem. Biol.* **10**, 658 (2006).
- [128] L. D. Jacobson and J. M. Herbert, *J. Am. Chem. Soc.* **132**, 10000 (2010).
- [129] R. Lugo and P. Delahay, *J. Chem. Phys.* **57**, 2122 (1972).
- [130] F.-Y. Jou and G. R. Freeman, *J. Phys. Chem.* **81**, 909 (1977).
- [131] F.-Y. Jou and G. R. Freeman, *Can. J. Chem.* **57**, 591 (1979).
- [132] A. Staib and D. Borgis, *J. Chem. Phys.* **103**, 2642 (1995).
- [133] S. S. Xantheas, C. J. Burnham, and R. J. Harrison, *J. Chem. Phys.* **116**, 1493 (2002).
- [134] G. S. Fanourgakis, E. Aprá, and S. S. Xantheas, *J. Chem. Phys.* **121**, 2655 (2004).
- [135] A. DeFusco, D. Schofield, and K. D. Jordan, *Mol. Phys.* **105**, 2681 (2007).
- [136] F. Wang and K. D. Jordan, *J. Chem. Phys.* **114**, 10717 (2001).
- [137] J. O. Hirschfelder, C. F. Curtiss, and R. B. Bird, *Molecular Theory of Gases and Liquids* (John Wiley, New York, 1954).
- [138] J. Xu and K. D. Jordan, *J. Phys. Chem. A* **114**, 1364 (2010).
- [139] J. M. Herbert and M. Head-Gordon, *Phys. Chem. Chem. Phys.* **8**, 68 (2006).
- [140] C. F. Williams and J. M. Herbert, *J. Phys. Chem. A* **112**, 6171 (2008).
- [141] K. Yagi, Y. Okano, Y. Kawashima, T. Tsudeda, and K. Hirao, *J. Phys. Chem. A* **112**, 9845 (2008).
- [142] T. H. Choi and K. D. Jordan, *Chem. Phys. Lett.* **464**, 139 (2008).
- [143] E. R. Davidson, S. A. Hagstrom, S. J. Chakravorty, V. M. Umar, and C. F. Fischer, *Phys. Rev. A* **44**, 7071 (1991).
- [144] G. K.-L. Chan and M. Head-Gordon, *J. Chem. Phys.* **118**, 8551 (2003).
- [145] P. M. Hare, E. A. Price, C. M. Stanisky, I. Janik, and D. M. Bartels, *J. Phys. Chem. A* **114**, 1766 (2010).
- [146] J. L. McHale, *Molecular Spectroscopy* (Prentice Hall, Englewood Cliffs, NJ, 1999).
- [147] I. A. Shkrob, *J. Phys. Chem. A* **110**, 3967 (2006).
- [148] I. A. Shkrob, *J. Phys. Chem. A* **111**, 5223 (2007).
- [149] I. A. Shkrob, W. J. Glover, R. E. Larsen, and B. J. Schwartz, *J. Phys. Chem. A* **111**, 5232 (2007).
- [150] A. E. Reed, R. B. Weinstock, and F. Weinhold, *J. Chem. Phys.* **83**, 735 (1985).
- [151] F. Weinhold, in *Encyclopedia of Computational Chemistry*, edited by P.v.R Schleyer, N. L. Allinger, T. Clark, J. Gastieger, P. A. Kollman, H. F. Schaefer III, and P. R. Schreiner (John Wiley, Chichester, 1999), Vol. 3, pp. 1792–1811.
- [152] J. M. Herbert and M. Head-Gordon, *J. Am. Chem. Soc.* **128**, 13932 (2006).
- [153] J. R. Roscioli, N. I. Hammer, M. A. Johnson, K. Diri, and K. D. Jordan, *J. Chem. Phys.* **128**, 104314 (2008).
- [154] M.E. Casida, in *Recent Advances in Density Functional Methods, Part I*, edited by D. P. Chong, volume I of *Recent Advances in Computational Chemistry* (World Scientific, River Edge, NJ, 1995), chapter 5, pp. 155–192.
- [155] A. Dreuw and M. Head-Gordon, *Chem. Rev.* **105**, 4009 (2005).
- [156] L. Bernasconi, M. Sprik, and J. Hutter, *J. Chem. Phys.* **119**, 12417 (2003).

- [157] J. Neugebauer, M. J. Louwerse, E. J. Baerends, and T. A. Wesolowski, *J. Chem. Phys.* **122**, 094115 (2005).
- [158] A. Lange and J. M. Herbert, *J. Chem. Theory Comput.* **3**, 1680 (2007).
- [159] A. Dreuw, J. L. Weisman, and M. Head-Gordon, *J. Chem. Phys.* **119**, 2943 (2003).
- [160] A. W. Lange, M. A. Rohrdanz, and J. M. Herbert, *J. Phys. Chem. B* **112**, 6304 (2008).
- [161] A. W. Lange and J. M. Herbert, *J. Am. Chem. Soc.* **131**, 3913 (2009).
- [162] M. A. Rohrdanz and J. M. Herbert, *J. Chem. Phys.* **129**, 034107 (2008).
- [163] H. Iikura, T. Tsuneda, T. Yanai, and K. Hirao, *J. Chem. Phys.* **115**, 3540 (2001).
- [164] Y. Tawada, T. Tsuneda, S. Yanagisawa, T. Yanai, and K. Hirao, *J. Chem. Phys.* **120**, 8425 (2004).
- [165] J.-W. Song, T. Hirose, T. Tsuneda, and K. Hirao, *J. Chem. Phys.* **126**, 154105 (2007).
- [166] T. Sato, T. Tsuneda, and K. Hirao, *J. Chem. Phys.* **126**, 234114 (2007).
- [167] T. Yanai, D. P. Tew, and N. C. Handy, *Chem. Phys. Lett.* **393**, 51 (2004).
- [168] O. A. Vydrov and G. E. Scuseria, *J. Chem. Phys.* **125**, 234109 (2006).
- [169] T. M. Henderson, B. G. Janesko, and G. E. Scuseria, *J. Chem. Phys.* **128**, 194105 (2008).
- [170] T. M. Henderson, B. G. Janesko, and G. E. Scuseria, *J. Phys. Chem. A* **112**, 12530 (2008).
- [171] J.-D. Chai and M. Head-Gordon, *J. Chem. Phys.* **128**, 084106 (2008).
- [172] M. A. Rohrdanz, K. M. Martins, and J. M. Herbert, *J. Chem. Phys.* **130**, 054112 (2009).
- [173] R. Baer, E. Livshits, and U. Salzner, *Annu. Rev. Phys. Chem.* **61**, 85 (2010).
- [174] Y. Shao, L. Fusti-Molnar, Y. Jung, J. Kussmann, C. Ochsenfeld, S. T. Brown, A. T. B. Gilbert, L. V. Slipchenko, S. V. Levchenko, D. P. O'Neill, R. A. DiStasio Jr, R. C. Lochan, T. Wang, G. J. O. Beran, N. A. Besley, J. M. Herbert, C. Y. Lin, T. Van Voorhis, S. H. Chien, A. Sodt, R. P. Steele, V. A. Rassolov, P. E. Maslen, P. P. Korambath, R. D. Adamson, B. Austin, J. Baker, E. F. C. Byrd, H. Dachsel, R. J. Doerksen, A. Dreuw, B. D. Dunietz, A. D. Dutoi, T. R. Furlani, S. R. Gwaltney, A. Heyden, S. Hirata, C.-P. Hsu, G. Kedziora, R. Z. Khalliulin, P. Klunzinger, A. M. Lee, M. S. Lee, W. Liang, I. Lotan, N. Nair, B. Peters, E. I. Proynov, P. A. Pieniazek, Y. M. Rhee, J. Ritchie, E. Rosta, C. D. Sherrill, A. C. Simmonett, J. E. Subotnik, H. L. Woodcock III, W. Zhang, A. T. Bell, A. K. Chakraborty, D. M. Chipman, F. J. Keil, A. Warshel, W. J. Hehre, H. F. Schaefer III, J. Kong, A. I. Krylov, P. M. W. Gill, and M. Head-Gordon, *Phys. Chem. Chem. Phys.* **8**, 3172 (2006).
- [175] A. D. Becke, *Phys. Rev. A* **38**, 3098 (1988).
- [176] T. Tsuneda, T. Suzumura, and K. Hirao, *J. Chem. Phys.* **110**, 10664 (1999).
- [177] A. V. Luzanov, A. A. Sukhorukov, and V. E. Umanskii, *Theor. Exp. Chem.* **10**, 354 (1976).
- [178] R. L. Martin, *J. Chem. Phys.* **118**, 4775 (2003).
- [179] I. Mayer, *Chem. Phys. Lett.* **437**, 284 (2007).
- [180] J. S. Townsend, *A Modern Approach to Quantum Mechanics* (McGraw-Hill, New York, 1992).
- [181] A. Khan, *J. Chem. Phys.* **125**, 024307 (2006).
- [182] T. Frigato, J. VandeVondele, B. Schmidt, C. Schütte, and P. Jungwirth, *J. Phys. Chem. A* **112**, 6125 (2008).
- [183] M. Gutowski and P. Skurski, *J. Phys. Chem. B* **101**, 9143 (1997).
- [184] S. F. Boys, *Rev. Mod. Phys.* **32**, 296 (1960).
- [185] T. James, D. J. Wales, and J. Hernández-Rojas, *Chem. Phys. Lett.* **415**, 302 (2005).
- [186] J. V. Coe, *J. Phys. Chem. A* **101**, 2055 (1997).
- [187] H. M. Lee, S. B. Suh, P. Tarakeshwar, and K. S. Kim, *J. Chem. Phys.* **122**, 044309 (2005).
- [188] H. J. C. Berendsen, J. P. M. Postma, W. F. van Gunsteren, and J. Hermans, in *Intermolecular Forces*, edited by B. Pullman (North Holland, Dordrecht, 1981), pp. 331–342.
- [189] K. Toukan and A. Rahman, *Phys. Rev. B* **31**, 2643 (1985).
- [190] D. J. Wales and J. P. K. Doyle, *J. Phys. Chem. A* **101**, 5111 (1997).
- [191] H. Kabrede and R. Hentschke, *J. Phys. Chem. B* **107**, 3914 (2003).
- [192] M. Boero, M. Parrinello, K. Terakura, T. Ikeshoji, and C. C. Liew, *Phys. Rev. Lett.* **90**, 226403 (2003).

- [193] P. Ren and J. W. Ponder, *J. Phys. Chem. B* **107**, 5933 (2003).
- [194] P. Ren and J. W. Ponder, *J. Phys. Chem. B* **108**, 13427 (2004).
- [195] J. W. Ponder, C. Wu, P. Ren, V. S. Pande, J. D. Chodera, M. J. Schnieders, I. Haque, D. L. Mobley, D. S. Lambrecht, R. A. DiStasio Jr, M. Head-Gordon, G. N. I. Clark, M. E. Johnson, and T. Head-Gordon, *J. Phys. Chem. B* **114**, 2549 (2010).
- [196] B. Thole, *Chem. Phys.* **59**, 341 (1981).
- [197] M. A. Morrison and L. A. Collins, *Phys. Rev. B* **17**, 918 (1978).
- [198] M. H. Cohen and V. Heine, *Phys. Rev.* **122**, 1821 (1961).
- [199] J. Schnitker and P. J. Rossky, *J. Chem. Phys.* **131**, 037102 (2009).
- [200] J. R. R. Verlet, A. E. Bragg, A. Kammrath, O. Cheshnovsky, and D. M. Neumark, *Science* **310**, 1769 (2005).
- [201] L. Turi, W.-S. Sheu, and P. J. Rossky, *Science* **310**, 1769 (2005).
- [202] A. Gaathon, G. Czapski, and J. Jortner, *J. Chem. Phys.* **58**, 2648 (1973).
- [203] K. H. Schmidt, P. Han, and D. M. Bartels, *J. Phys. Chem.* **99**, 10530 (1995).
- [204] N. Agmon, *Chem. Phys. Lett.* **244**, 456 (1995).
- [205] M. Tuckerman, K. Laasonen, M. Sprik, and M. Parrinello, *J. Phys. Chem.* **99**, 5749 (1995).
- [206] L. D. Jacobson and J. M. Herbert, *J. Chem. Phys.* **133**, 154506 (2010).
- [207] G. Makov and A. Nitzan, *J. Phys. Chem.* **98**, 3459 (1994).
- [208] J. Kongsted, A. Osted, K. V. Mikkelsen, and O. Christiansen, *Mol. Phys.* **100**, 1813 (2002).
- [209] J. Kongsted, A. Osted, K. V. Mikkelsen, and O. Christiansen, *J. Chem. Phys.* **118**, 1620 (2003).
- [210] C. B. Nielsen, O. Christiansen, K. V. Mikkelsen, and J. Kongsted, *J. Chem. Phys.* **126**, 154112 (2007).
- [211] S. Yoo, F. Zahariev, S. Sok, and M. S. Gordon, *J. Chem. Phys.* **129**, 144112 (2008).
- [212] P. Arora, L. V. Slipchenko, S. P. Webb, A. DeFusco, and M. S. Gordon, *J. Phys. Chem. A* **114**, 6742 (2010).
- [213] L. V. Slipchenko, *J. Phys. Chem. A* **114**, 8824 (2010).
- [214] A. T. B. Gilbert, N. A. Besley, and P. M. W. Gill, *J. Phys. Chem.* **112**, 13164 (2008).
- [215] N. A. Besley, A. T. B. Gilbert, and P. M. W. Gill, *J. Chem. Phys.* **130**, 124308 (2009).
- [216] L. Mones and L. Turi, *J. Chem. Phys.* **132**, 154507 (2010).
- [217] M. Assel, R. Laenen, and A. Laubereau, *J. Phys. Chem. A* **102**, 2256 (1998).
- [218] M. Assel, R. Laenen, and A. Laubereau, *J. Chem. Phys.* **111**, 6869 (1999).
- [219] M. C. Cavanagh, I. B. Martini, and B. J. Schwartz, *Chem. Phys. Lett.* **396**, 359 (2004).
- [220] D. H. Son, P. Kambhampati, T. W. Kee, and P. F. Barbara, *J. Phys. Chem. A* **105**, 8269 (2001).
- [221] B. Boudaïffa, P. Cloutier, D. Hunting, M. A. Huels, and L. Sanche, *Science* **287**, 1658 (2000).
- [222] M. A. Huels, B. Boudaïffa, P. Cloutier, D. Hunting, and L. Sanche, *J. Am. Chem. Soc.* **125**, 4467 (2003).
- [223] J. Simons, *Acc. Chem. Res.* **39**, 772 (2006).
- [224] X. Chen and S. E. Bradforth, *Annu. Rev. Phys. Chem.* **59**, 203 (2008).
- [225] M. Haranczyk and M. Gutowski, *J. Chem. Theory Comput.* **4**, 689 (2008).
- [226] W. Humphrey, A. Dalke, and K. Schulten, *J. Molec. Graphics* **14**, 33 (1996).